České vysoké učení technické v Praze
Fakulta Elektrotechnická

DIPLOMOVÁ PRÁCE

2005 **Ondřej Holub**

České vysoké učení technické v Praze
Fakulta Elektrotechnická

DIPLOMOVÁ PRÁCE

Ondřej Holub

2005

České vysoké učení technické v Praze
Fakulta elektrotechnická
Katedra řídicí techniky

DIPLOMOVÁ PRÁCE

Tool Developement for VLT Telescope Controller Design

Ondřej Holub

2005

Autor: Ondřej Holub

Vedoucí: Ing. Zdeněk Hurák, Ph.D.
Centrum aplikované kybernetiky, Katedra řídicí techniky,
Fakulta elektrotechnická, České vysoké učení technické v Praze

Oponent: Ing. Jaromír Fišer, Ph.D.
Centrum aplikované kybernetiky, Ústav přístrojové a řídicí techniky,
Fakulta strojní, České vysoké učení technické v Praze

Rok: 2005

Anotace

Moderní teleskopy, jako například Very Large Telescope (VLT) v Chile, vyžadují velmi přesné polohování optické soustavy a současně rychlou odezvu polohovacího zařízení na požadavky operátora. Přitom s narůstajícími rozměry teleskopů získává na významu také potlačení vlivu poryvů větru na přesnost a stabilitu polohování. Tato práce se zabývá přesnější formulací zmíněných požadavků z hlediska návrhu řídicího algoritmu a poukazuje na to, že jsou tyto požadavky zčásti konfliktní. Pro dodaný dynamický model VLT teleskopu je navržen regulátor pomocí $\mathcal{H}_\infty$ optimalizace. Navržený regulátor ve sledovaných parametrech překonává stávající řešení. Cenou za toto zlepšení je zvýšený řád regulátoru. Při využití $\mathcal{H}_\infty$ optimalizace vůbec se často setkáváme s dynamickými modely vysokého řádu, které komplikují proces návrhu. Proto jako součást práce byl vytvořen i nástroj pro pohodlný přístup k metodám redukce řádu modelu v prostředí Matlab. Praktická použitelnost $\mathcal{H}_\infty$ optimalizace je demonstrována na laboratorním experimentu polohování pružného ramene na otočném kloubu.

Abstract

Modern telescopes, such as the Very Large Telescope (VLT) in Chile, require very precise positioning of the optical system and fast response to reference signal at the same time. On the other hand enlargements in the telescope size increase the importance of wind disturbance attenuation. This work precisely formulates the mentioned control objectives and points out that these objectives are somewhat conflicting. For the given dynamical model of the VLT, controller is designed utilizing $\mathcal{H}_\infty$ synthesis. The resulting controller is superior to the existing solution, however, it has relatively high system order. Higher order models are rather common within the $\mathcal{H}_\infty$ synthesis, thus a tool for comfortable access to reduction methods has been implemented in Matlab. Finally, practical aspects of $\mathcal{H}_\infty$ synthesis are shown on an exmple of flexible link positioning.

Prohlášení

Prohlašuji, že jsem zadanou diplomovou práci vypracoval samostatně s přispěním vedoucího diplomové práce a použil jsem pouze literaturu v práci uvedenou.

Nemám závažný důvod proti užití tohoto školního díla ve smyslu 60 Zákona č. 121/2000 Sb., o právu autorském, o právech souvisejících s právem autorským a o změně některých zákonů (autorský zákon).

V Praze dne 27. ledna 2005 Ondřej Holub

Acknowledgements

I would foremost like to thank my family and my parents especially for the unconditional support and love they have given me throughout my life.

I would also like to express my sincere gratitude to my thesis advisor and an excellent teacher, Zdeněk Hurák, for his assistance during the work on this thesis.

Furthermore, I would like to thank my colleagues, in particular Petr Augusta, for their support that has always come in the right time.

Finally, I would like to thank Kristína Benkovičová, who has shown me, how kind and empathetic one can be.

Contents

Chapter 1

Introduction

This diploma thesis has been motivated by the control problem of the *Very Large Telescope* (VLT) run by European Southern Observatory at Cerro Paranal, Chile. The VLT is a complex structure with highly pronounced resonant frequencies. In addition, these resonances are activated by wind buffets.

Recently, there have been efforts to further improve control of the VLT so as to obtain higher attenuation of the disturbant wind. To do so, the existing 2-loop PI controller has been tuned. Limited performance of the classical approach has lead to efforts to design a new controller using modern advanced control techniques. The $\mathcal{H}_\infty$ synthesis has been considered as an appropriate one. Reason for this is that $\mathcal{H}_\infty$ synthesis is able to give a controller, that can be easily implemented into the currently used control scheme.

In context of the presented search for a better controller, the goal of this work has been to create a background for an $\mathcal{H}_\infty$ controller design. On the one hand to create a graphical user interface (GUI) for a comfortable design of an $\mathcal{H}_\infty$ controller in Matlab and on the other to design one such controller for the VLT. The GUI should simplify the design procedure and should consist of two components - one for model order reduction and one for the actual $\mathcal{H}_\infty$ design.

At the beginning it was expected that the time schedule of the work would should be as follows. At first, several attempts to design a suitable controller for the VLT should be performed. Consequently, the software tools for $\mathcal{H}_\infty$ design should be developed. During the time it has become clear that the $\mathcal{H}_\infty$ design procedure is much more complicated than it was expected to be. Moreover, algorithms for $\mathcal{H}_\infty$ design implemented in Matlab have been evaluated as immature for an automatic design procedure.

At the same time laboratory model for Quanser Rotary Experiment[Quanser] was bought. This was considered as an opportunity to experimentaly verify the $\mathcal{H}_\infty$ controller design and gather new experience in the field. Thus, only the GUI for model order reduction has been realized. Instead of developing GUI for $\mathcal{H}_\infty$ design the Rotary Experiment has been undertaken.

The layout of this document is as follows. Chapter 2 briefly summarizes the controller design based on minimization of $\mathcal{H}_\infty$ norms of the closed-loop transfer functions. Aspects of this approach important for the VLT control problem are discussed in detail. Also

properties of the used state-space algorithm implemented in Robust Control Toolbox for Matlab [6] are mentioned.

Chapter 3 describes the GUI for model order reduction. It gives a description of model order reduction methods available within the Matlab Release 13 package [Matlab]. Consequently, it is gone through the GUI and the use of the GUI is shown on an example.

Chapter 4 is devoted to the respective VLT Telescope position control. The VLT control problem is introduced and its main aspects are discussed. A frequency-domain formulation of the control goals is stated and suitable controller is found using the $\mathcal{H}_\infty$ synthesis methods. At last, the results are compared to the existing solution.

Chapter 5 copes with the Quanser Rotary Experiment. The Rotary Experiment states for the developement of a controller for a flexible link attached to a DC motor. It is shown that such plant suffers from vibrations in an analogous way to the aforementioned VLT telescope system. This is the reason why the Rotary Experiment has been chosen - as an opportunity to prove the worth of $\mathcal{H}_\infty$ synthesis on an accessible laboratory system. Thus it is possible to go through the whole identification procedure and learn more about weaknesses and limitations of the plant model that are imposed by necessary simplifications done during this process.

Finally, Chapter 6 gives a conclusion of the contributions of this thesis.

Chapter 2

$\mathcal{H}_\infty$ Synthesis in a Nutshell

This chapter goes through the basics of $\mathcal{H}_\infty$ control. It formulates the $\mathcal{H}_\infty$ control problem and depicts important properties of the state-space algorithm used to solve this problem.

2.1 Introduction

Consider a plant with transfer function P. A typical control problem is to fulfill some requirements set on the plant using a feedback controller C (see Figure 2.1). The controller changes value of the plant's input according to the difference between the required value r and the measured output y of the plant.

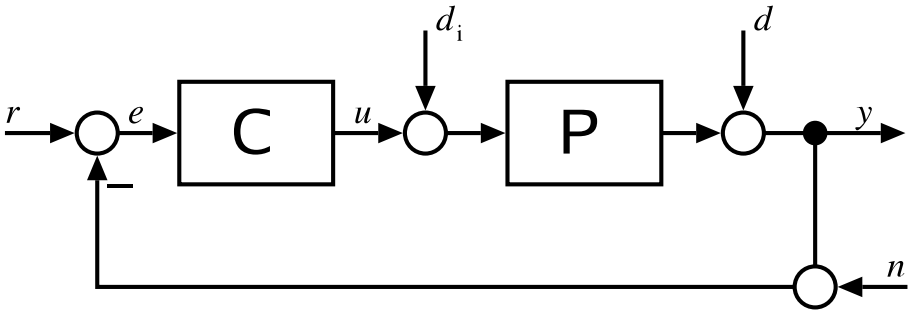

Figure 2.1: Typical closed-loop system

Measurement of the output y contains sensor noise and usually external disturbances enter the closed-loop system at the plant input and (or) output. Moreover the plant model P is uncertain. This is caused partly by the simplifiactions done during modelling and identification of P, partly by the change of plant parameters during its operation.

To design a controller C, that satisfies all the requirements set on the system and that is robust to plant uncertainty, it is possible to employ $\mathcal{H}_\infty$ synthesis methods. $\mathcal{H}_\infty$ methods search for a controller C, that stabiliezis the closed-loop system and minimizes

$\mathcal{H}_\infty$ norm of a particular matrix function which comprises of weighted closed-loop transfer functions.

In order to make the use of $\mathcal{H}_\infty$ synthesis feasible, it is necessary to formulate control goals in the frequency domain. Section 2.2 shows how to do that. Control goals cannot be arbitrary and Section 2.3 goes through the limits of performance. Next section describes the state-space algorithm of $\mathcal{H}_\infty$ synthesis implemented in Robust Control Toolbox for Matlab [6] and used within this work. The algorithm's limitations are mentioned and some ways how to get over them are proposed. Section 2.5 demonstrates the $\mathcal{H}_\infty$ design on an example. Finally, Section 2.6 concludes this chapter.

2.2 $\mathcal{H}_\infty$ Formulation of a Control Problem

In order to specify a control problem in a way suitable for $\mathcal{H}_\infty$ synthesis, let us summarize typical control objectives at first. Typical objectives of the controller design are: to assure internal stability of the closed-loop system subject to plant uncertainty, to obtain swift and smooth time response on typical reference commands, to minimize the effects of disturbances and noise on the plant's output and not to exceed saturation bounds of the controller output. All the control goals need to be satisfied simultanously.

These control goals can be transformed into requirements on some closed-loop transfer functions. To do so, we need to introduce them. Consider the system of Figure 2.1 once again. Define the closed-loop sensitivity S, complementary sensitivity T and input sensitivity U as follows (cf. [10, 19, 29]). Let S be the transfer function from reference r to controller input e, let T be the transfer from reference r to output y and let U be the transfer from reference r to controller output u. For the purposes of the VLT controller design the transfer function D from input disturbance d_i to output y is needed. In [12] D is reffered to as disturbance sensitivity. For the system of Figure 2.1 S, T, U and D can be evaluated as

$$\begin{aligned} S &= \frac{1}{1+P\,C} \\ T &= \frac{P\,C}{1+P\,C} \\ U &= \frac{C}{1+P\,C} \\ D &= \frac{P}{1+P\,C}. \end{aligned} \tag{2.1}$$

To evaluate the requirements set on the closed-loop transfer functions some norm needs to be introduced. $\mathcal{H}_\infty$ formulation of control problems uses the induced operator norm $\mathcal{H}_\infty$ [10]. Note that the name of $\mathcal{H}_\infty$ synthesis is derived from the name of this norm. The $\mathcal{H}_\infty$ norm of a continous-time transfer function G is

$$\|G(j\,\omega)\|_\infty = \sup_{\omega\in\mathbb{R}} |G(j\,\omega)|.$$

Generally, the $\mathcal{H}_\infty$ norm of a transfer function G, $\|G(j\,\omega)\|_\infty$, is equal to the largest singular value of G (the largest eigenvalue of $G^{\mathrm{T}}\,G$), if it is finite. In the SISO case, $\|G(j\,\omega)|_\infty$ is equal to the peak value of the amplitude Bode plot.

As the $\mathcal{H}_\infty$ norm has been introduced, the control goals can be formulated using the $\mathcal{H}_\infty$ norm of appropriate closed-loop transfer functions, namely [33]:

1. For disturbance rejection make $\|S\|_\infty$ or $\|D\|_\infty$ small.
2. For noise attenuation make $\|T\|_\infty$ small.
3. For good reference tracking make $\|T\|_\infty \approx 1/\|T\|_\infty \approx 1$.
4. For avoidance of control signal saturation make $\|U\|_\infty$ small.

Note that the frequency domain formulation of control goals does not neccesarily result in a request to minimize the closed-loop functions in the whole frequency range. On the contrary, each closed-loop function needs to be minimized in a specific frequency interval and with different intensity. To do so, frequency-dependent weights need to be introduced to the closed-loop system.

Consider the SISO closed-loop system of Figure 2.2. Addition of the weights W_1, W_2, W_3 and W_4 to the closed-loop system (taken from Figure 2.1) has modified the functions S, T, U and D. The new closed-loop transfers are

$$\begin{aligned} S' &= W_1\,S = \frac{W_1}{1+P\,C}, \\ T' &= W_3\,T = \frac{W_3\,P\,C}{1+P\,C}, \\ U' &= W_2\,U = \frac{W_2\,C}{1+P\,C}, \\ D' &= W_3\,D\,W_4 = \frac{W_3\,P\,W_4}{1+P\,C}. \end{aligned} \tag{2.2}$$

Using appropriate weights W_1, W_2, W_3 and W_4 it is possible to formulate the requirements on the closed-loop functions S, U, T and D, simply as a simultaneous minimization of the norms $\|W_1\,S\|_\infty$, $\|W_2\,U\|_\infty$, $\|W_3\,T\|_\infty$ and $\|W_3\,D\,W_4\|_\infty$.

Internal stabilization of a closed-loop system will be discussed now. A closed-loop system is internaly stable iff all the transfer functions within this system are stable [10]. For the system of Figure 2.1 this states for the stability of S, T, U and D. Stability of the closed-loop system with an uncertain plant P can be evaluated using the Small Gain Theorem (SGT) [29, 36]. Consider the closed-loop system in Figure 2.3a. Let Δ be an arbitrary transfer function with the $\mathcal{H}_\infty$ norm $\|\Delta\|_\infty < 1$. Then the closed-loop system is stable iff $\|M\|_\infty \leq 1$.

Now let the uncertainty of P be described by a multiplicative model,

$$P(j\,\omega) = P_0(j\,\omega)\,(1 + \Delta(j\,\omega)\,W_3(j\,\omega)), \tag{2.3}$$

where $\|\Delta\|_\infty < 1$ is arbitrary, P_0 is a nominal plant and W_3 is a frequency-dependent weight. Closed-loop system with multiplicative model of uncertainty of P is shown in

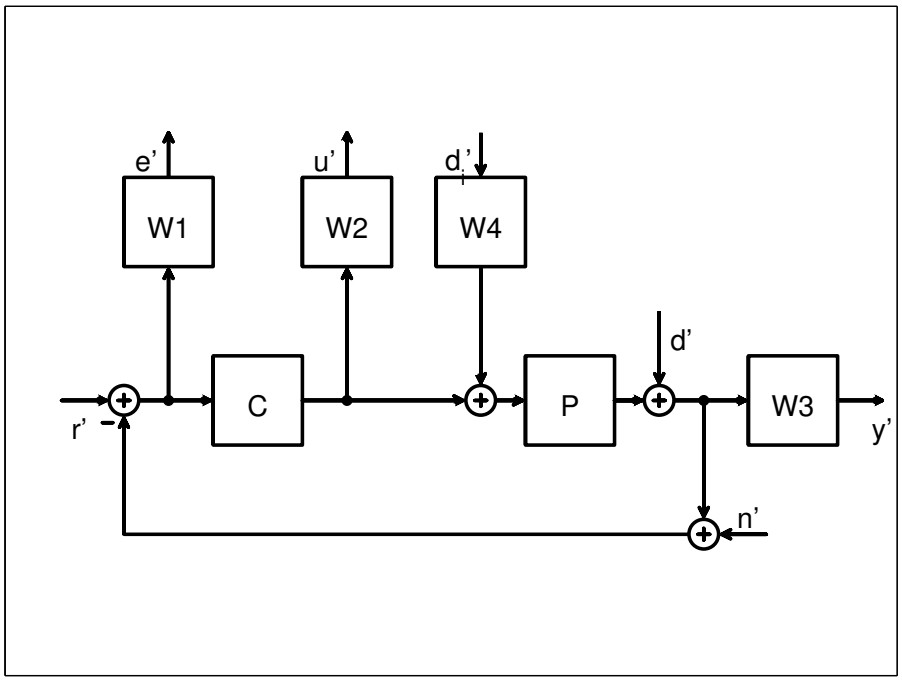

Figure 2.2: Setup for the $\mathcal{H}_\infty$ formulation of a control problem

Figure 2.3b. According to the SGT this closed-loop system is internaly stable iff

$$\|M(j\,\omega)\|_\infty = \|W_3(j\,\omega)\,T_0(j\,\omega)\|_\infty \leq 1,$$

where

$$T_0(j\,\omega) = \frac{P_0(j\,\omega)\,C(j\,\omega)}{1 + P_0(j\,\omega)\,C(j\,\omega)}$$

is the nominal complementary sensitivity function.

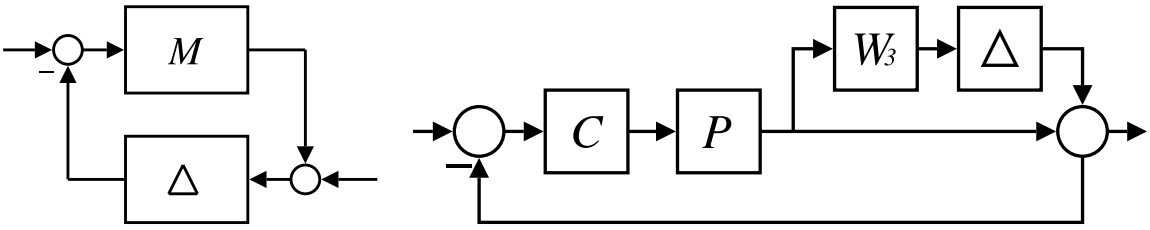

(a) (b)

Figure 2.3: Setup for the Small Gain Theorem (a) and closed-loop system with multiplicative model of uncertainty of P (b)

Remark that three different bounds on the complementary sensitivity T have been introduced. One for noise attenuation, another for reference tracking and at last one for robust stability of the closed-loop system. Note that these objectives are conflicting, e.g. noise attenuation needs T to be small, while good reference tracking results in $T \approx 1$. Many other conflicts can be found analyzing all the closed-loop requirements [7, 29,

33]. Feedback design is therefore a trade-off over frequency objectives. Next section goes through typical frequency-dependent requirements on S, T, U and D and summarizes limitations that a feasible set of control goals must fulfill.

2.3 Weight Selection and Limits of Performance

Now the control objectives will be described in more detail to see what kinds of weighting filters are appropriate to formulate the control goals.

At first, reconsider the multiplicative model of uncertainty (2.3). Typically, the model uncertainty caused by dynamics neglecting becomes significant in high frequency range. Thus the relative model error W_3

$$W_3 = \frac{P}{P_0} - 1 \tag{2.4}$$

increases with the increasing frequency and T needs to be made small in the high frequency region.

Now consider the reference tracking. For a perfect reference tracking one would need T to be identically equal to one in the whole frequency range. Except many other problems, this would lead to instability due to (always present) uncertainty of the plant P. Fortunately, for a good reference tracking it is sufficient to have $T \approx 1$ only for $\omega \leq \omega_0$. For $\omega \geq \omega_0$, T should roll-off smoothly. The value of ω_0 is different from case to case.

Inspection of (2.1) gives that for arbitrary C and P the following equality holds

$$S + T = 1. \tag{2.5}$$

Thus reference tracking requires $S \approx 0$ in the low frequency region. Moreover, based on properties of the Laplace transform, it can be shown [19, 29] that for an asymptotic tracking of type-k reference command the sensitivity S needs to have $k + 1$ zeros at zero frequency. The type-k reference command is a signal with amplitude that can be bounded in the following way

$$|r(t)| \leq K\, t^k,$$

where $k = 0, 1, \ldots$ and $K > 0$.

Disturbance rejection expects either S or D to be small. Note that D can be expressed as

$$D = S\, P, \tag{2.6}$$

so rejection of the input disturbance can be expressed in terms of requirements set on S. Because of the needed robust stability and the link between S and T (2.5), rejection of disturbances is (in a general case) possible only in the low frequency region.

Attenuation of noise is bound with the complementary sensitivity T. It is of no surprise, that noise can be attenuated only in the high frequency region. Low frequency noise (such as hum) cannot be mitigated by means of feedback.

Finally, to prevent the control signal from saturation, the input sensitivity u should be made small. Usually it is sufficient to bound u with a simple all-pass gain.

Summarizing the mentioned requirements set on both S and T, it is obvious, that T should behave as a low-pass filter while S should behave as a high-pass filter. In the most cases a bound set on u is an all-pass filter and a shape expected for d can be derived according to (2.6).

To shape the closed-loop transfer functions, weighting filters are used [7, 29]. Usually the weighting filters are desrcibed by the parameters M, k, ω_1 and ϵ (Figure 2.4). M is the maximal value of peaks of the weighted function, k is the the filter order, ω_1 defines the filter bandwidth ($W(\omega_1) = 1$) and ϵ states for the minimal attenuation in the stopband. It is possible to find a stable weighting filter with real poles and zeros that exactly matches specification

$$W_R(s) = \left[\frac{a\,s + b}{s + c}\right]^k,$$

where

$$\begin{aligned} a &= \sqrt[k]{M}, \\ b &= c\sqrt[k]{\epsilon}, \\ c &= \omega_1 \sqrt{\frac{\sqrt[k]{M^2} - 1}{1 - \sqrt[k]{\epsilon^2}}} \end{aligned}$$

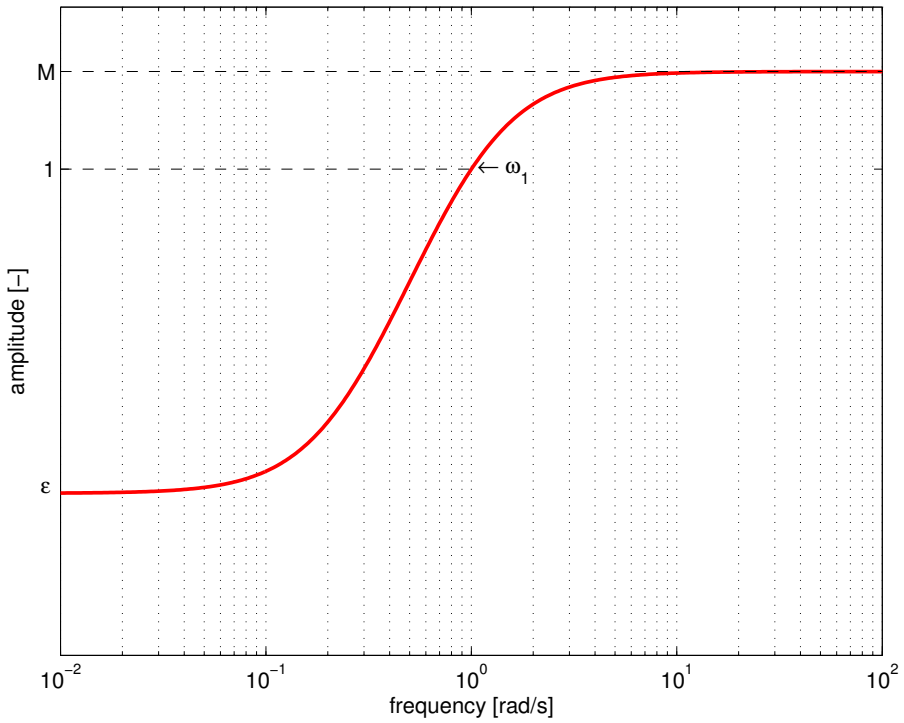

Figure 2.4: Parameters of the weighting filters

Sometimes it can be advantageous to use a filter with pair of complex roots (e.g. when steep roll-off is needed near the transient frequency)

$$W_C(s) = \frac{k\,\omega_n^2}{s^2 + 2\xi\,\omega_n\,s + \omega_n^2}.$$

The roll-off near ω_1 is determined by the damping coefficient ξ. If $\xi > 1/\sqrt{2}$ the $W_C(s)$ peaks at the frequency $\omega_M = \omega_n\,\sqrt{1 - 2\,\xi^2}$ and the peak has value

$$M = \frac{k}{2\xi\,\sqrt{1-\xi^2}}.$$

One possible way how to fit the frequency domain specifications on weighting filters has been proposed. Now the limits set on the specification itself will be discussed. There are three important limitations on the shape of sensitivity S and complementary sensitivity T. The algebraic constraint, that has been already mentioned (2.5), Bode's sensitivity integral and Freudenberg-Looze equality [7, 29].

Bode has shown that if the series connection $L = P\,C$ of the plant P and the controller C has at least two more poles than zeros the sensitivity function S satisfies

$$\int_0^\infty \log|S(j\,\omega)|\,\mathrm{d}\,\omega = \pi \sum_i \mathrm{Re}\{p_i\} \tag{2.7}$$

where p_i are right-half plane (RHP) poles of L [29]. At first suppose that L has no RHP poles. Then the integral over all frequencies of $\log|S|$ is zero. For the feedback control to be useful, $|S|$ needs to be less than 1 over an effective low-frequency band. Bode's sensitivity integral implies that this can be achieved only at the cost of peaking of S at high frequencies. This property of S is sometimes called *the waterbed effect*. In the case that RHP poles of L are present, the right hand side of (2.7) is greater than zero and the penalty for minimization of S at low frequencies becomes even more severe.

It is useful to derive a lower bound on the peak value of S so as to establish an insight into the waterbed effect. Typical requirements on S can be expressed using templates as in Figure 2.5 [12]. The approximation of $|S|$ exhibits k-order roll-off at frequencies under f_1, between f_1 and f_2 it has value of m, the peak value is M and beyond f_3 $|S|$ is set to 1. Then the peak value of S can be given as a function of the other parameters k, m, f_1, f_2 and f_3

$$\log(M) = \frac{k\,f_1 - \log(m)\,f_2}{f_3 - f_2}. \tag{2.8}$$

To demonstrate the waterbed effect, consider the requirements on S for the VLT control problem. In Chapter 4 it will be stated that the highest possible f_2 and the lowest possible m is sought under the following restrictions: f_3 is set to 8 Hz, M should not exceed cf. 6 dB. Reasonable value for f_1 is 0.1 Hz. According to (2.8), Figure 2.6 shows the dependence of M on f_2 and m. It is obvious that extension of the bandwidth (increase

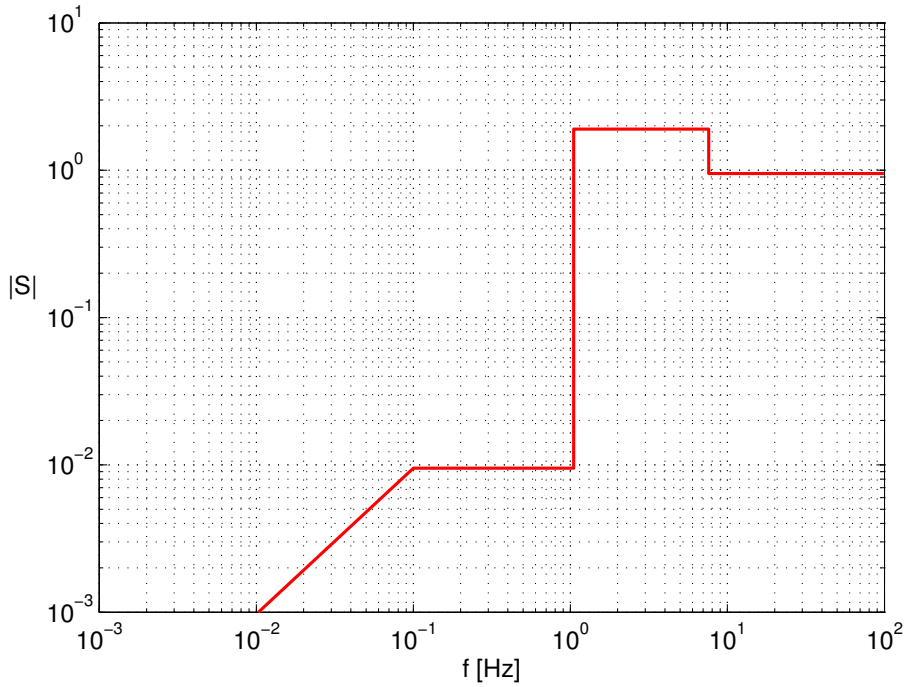

Figure 2.5: Template for a sensitivity function $log|S|$

in f_2) can be achieved only at the cost of peaking of $|S|$. To put it differently, the crossover region (i.e. the region between f_2 and f_3) cannot be arbitrarily narrow.

Freudenberg and Looze have further extended the Bode's results. A central result of their work is the Freudenberg-Looze equality [29]. Consider a stable closed-loop system with open-loop RHP zero $z = x + j\,y, x > 0$, then the sensitivity function S must satisfy

$$\int_0^\infty \log|S|\,\mathrm{d}\,W_z(\omega) = \pi\,\log|B(z)| \tag{2.9}$$

where $B(z)$ is the Blaschke product formed from the open-RHP poles p_i

$$B(z) = \frac{p_i - z}{\bar{p}_i + z}$$

and $W_z(\omega)$ is the phase of $(z + j\,\omega)/(z - j\,\omega)$. The quantity $\mathrm{d}\,W_z(\omega)$ may be viewed as a weighted length of the frequency integral and it equals the extra phase added by the RHP zero z over the frequency interval. The larger $\mathrm{d}\,W_z(\omega)$ is, the more the interval contributes to the right-hand side of (2.9). Thus the weighting function determines to what extent small values of $|S|$ at low frequencies need to be compensated by large values at high frequencies.

Analyzing a template similar to the one in Figure 2.5 it is possible to show that if the width of the band at which S may be made small is greater than the magnitude of the RHP zero z, the peak value of S assumes excessive values [29]. This holds for any RHP zero, in particular the one with smallest magnitude. Therefore, if excessive peaking of S is to be avoided, bandwidth of the closed-loop system cannot be extended beyond

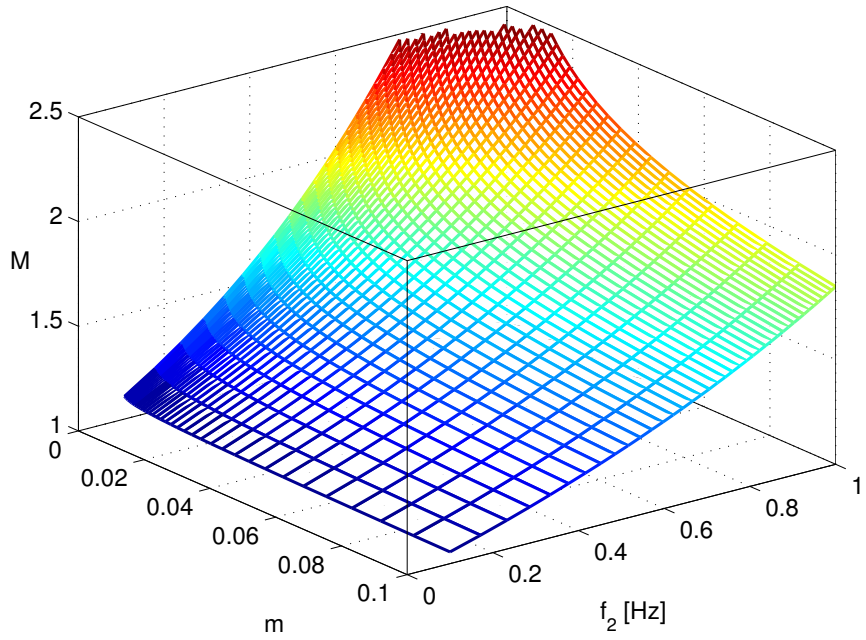

Figure 2.6: Dependence of the minimum achievable peak value M of sensitivity function on the bandwidth f_2 and attenuation m. The other parameters set to $f_1 = 0.1$ Hz, $f_3 = 8$ Hz.

the magnitude of the smallest RHP zero. $B(z)$ is replaced with 1 if there are no RHP poles. Otherwise, it is greater than 1. Hence, RHP poles make the plant more difficult to control. The situation gets even worse when a RHP pole is close to RHP zero and results in uncontrollable or unobservable unstable mode if they coincide.

In this section it has been summarized how to transform control objectives into the form suitable for $\mathcal{H}_\infty$ synthesis. That is, how to shape the weighting filters connected to the original closed-loop system. It has been pointed at the fact that control objectives are typically conflicting. Moreover, there are limitations that the closed-loop transfer functions must satisfy. Thus it is not trivial to formulate a feasible control specification. Usually it is relatively easy to shape the closed-loop transfer functions at very low and very high frequencies. The region, where all the conflicts happen, is the crossover region. Note that while requirements at both low- and high- frequency regions are clear, requirements at the crossover region are somewhat vague. As the crossover region is a key region for the closed-loop performance, the problem of weight selection is an iterative process. One starts with certain filters and adapts them in subsequent iterations so as they lead to a controller which gives acceptable behaviour of the closed-loop system. In the next section it is shown how to synthesize the controller based on the specification of weighting filters.

2.4 State-space Algorithm of the $\mathcal{H}_\infty$ Synthesis

Recall the formulation of the $\mathcal{H}_\infty$ control problem from previous sections: $\mathcal{H}_\infty$ control problem is a task to find controller C that simultanously stabilizes the closed-loop system and minimizes the frequency weighted norms of the closed-loop functions in (2.2). However, for the purposes of algorithms that solve the $\mathcal{H}_\infty$ problem, it is necessary to incorporate this formulation in the augmented plant framework.

The definition of an augmented plant is best done by means of a diagram shown in Figure 2.7. Notice that Figure 2.7 is just a reorganized closed-loop system from Figure 2.2 except that for simplicity the output disturbance d is not considered any longer. Nevertheless, the augmented plant of figure 2.3 is sufficient to formulate the VLT control problem. Loosely speaking, the augmented (or generalized) plant is *everything except for* C in Figure 2.2. The augmented plant has three inputs r, di and u and four outputs z_1, z_2, z_3 and y. The closed-loop controller C is connected to the augmented plant output y and drives the input u. Inputs r and d are driven by reference generator and external source of disturbances, respectively, and are reffered to as a vector w of external (or exogenous) inputs. The auxiliary outputs z_1, z_2 and z_3 have the meaning of control errors and ideally should be zero.

Let the matrix transfer function G of the augmented plant be partitioned as

$$\begin{pmatrix} z \\ y \end{pmatrix} = \begin{pmatrix} G_{11} & G_{12} \\ G_{21} & G_{22} \end{pmatrix} \begin{pmatrix} w \\ u \end{pmatrix}. \tag{2.10}$$

Then the closed-loop (matrix) transfer function H from external inputs w to the control

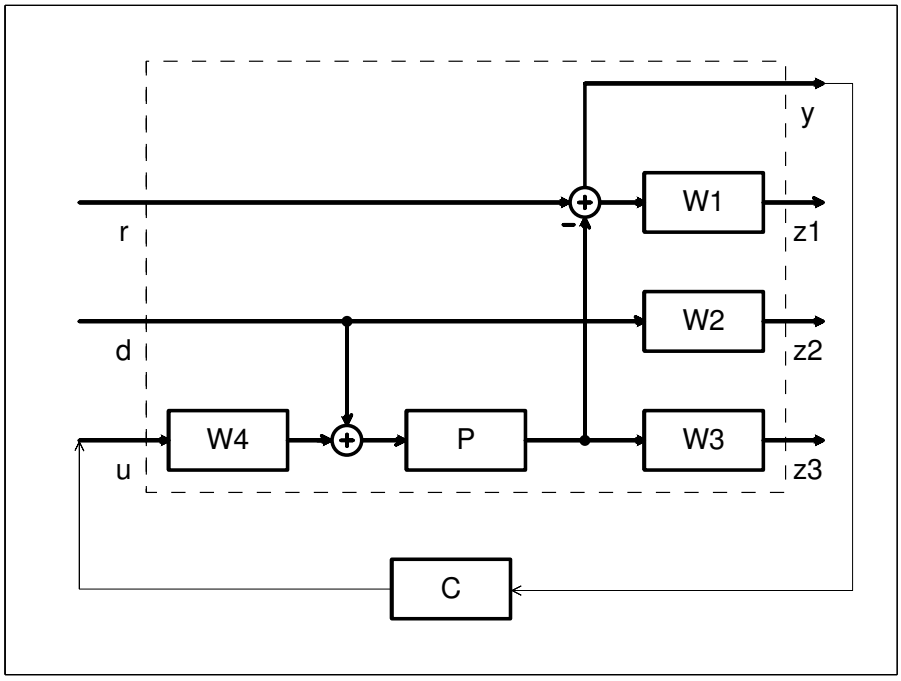

Figure 2.7: Augmented plant

error z is

$$H = G_{11} + G_{12}\, C\, (I - G_{22}\, K)^{-1}\, G_{21}. \tag{2.11}$$

Now the actual $\mathcal{H}_\infty$ control problem can be formulated. The standard $\mathcal{H}_\infty$ problem is the problem of determining a controller C that internally stabilizes the closed-loop system (as defined in 2.2) and minimizes the $\mathcal{H}_\infty$ norm of the closed-loop transfer matrix H (2.11) from external inputs w to the control error z [33], i.e.

$$\min_C \|H\|_\infty = \min_C \left\| \begin{pmatrix} W_1\, S & -W_1\, D\, W_4 \\ W_2\, U & -W_2\, T\, W_4 \\ W_3\, T & W_3\, D\, W_4 \end{pmatrix} \right\|_\infty \tag{2.12}$$

Note that there are two new components $-W_1DW_4$ and $-W_2TW_4$ in the matrix H, that have not been considered in (Section 2.2). These functions are the weighted transfers from input disturbance d_i to tracking error e and controller output u, respectively. The appereance of $-W_2TW_4$ in the matrix H subject to norm minimization can be understood so that request for simultaneous input disturbance attenuation (W_3DW_4) and controller output boundedness (W_2U) implicitely constraint influence of d_i on u. Explanation for the introduction of $-W_1DW_4$ is analogous.

Within this work, a state-space algorithm implemented in Robust Control Toolbox for Matlab [6] is used to solve the standard $\mathcal{H}_\infty$ problem. To come up with an explicit formula for an optimal solution C is generally very complicated if not impossible [29]. It is easier to solve the suboptimal problem, i.e. the problem whether or not there exists a stabilizing C that achieve $\|H\|_\infty < \gamma$ for some given bound $\gamma > 0$. A line search in γ then can bring us arbitrarily close to the optimal controller C_{opt}. This approach is called γ-iteration and is implemented in the Robust Control Toolbox [6] (as binary search).

There are two ways how to solve the standard problem – one in frequency domain and one based on state-space definition. The frequency domain solution is based on J-spectral factorization of particular matrix transfer function. Unfortunately, it is difficult to perform the J-spectral factorization when assuming higher-order or MIMO systems. Thus the state-space algorithm based on solution of two Ricatti equations is much more common.

For the user, it is not important what happens inside the algorithm. However, the user (controller designer) should be aware of the restrictions and assumptions on the augmented plant that need to be satisfied. Otherwise, the state-space algorithm fails. First, the state-space nomenclature will be introduced. Consider the augmented plant of Figure 2.7 once again. According to the partition of G in (2.11), the state-space model of the augmented plant is

$$\begin{aligned} \dot{x} &= A\, x + B_1\, w + B_2\, u, \\ z &= C_1\, x + D_{11}\, w + D_{12}\, u, \\ y &= C_2\, x + D_{21}\, w + D_{22}\, u. \end{aligned} \tag{2.13}$$

The assumptions on G are following ([7, 29, 33, 36]):

(A1) (A, B_2, C_2) is stabilizable and detectable
(A2) D_{12} and D_{21} have full rank
(A3) $\begin{pmatrix} A - j\,\omega\, I & B_2 \\ C_1 & D_{12} \end{pmatrix}$ has full column rank for all $\omega \in \mathbb{R}$
(A4) $\begin{pmatrix} A - j\,\omega\, I & B_1 \\ C_2 & D_{21} \end{pmatrix}$ has full row rank for all $\omega \in \mathbb{R}$

Assumption (A1) is precisely equivalent to the existence of controllers that internally stabilize the whole feedback system of Figure 2.7, not just the closed-loop transfer from u to y. Assumption (A2) is sufficient to ensure the controllers are proper and hence realizable. Assumptions (A3) and (A4) ensure that the optimal controller does not try to cancel poles or zeros on the imaginary axis which would result in closed-loop instability. Note that if $D_{12}^{\mathrm{T}}\, C_1 = B_1 D_{21}^{\mathrm{T}} = 0$, then (A3) and (A4) may be replaced with the assupmtion of stablizable and detectable (A, B_1, C_1).

It is clear that for most practical situations both the assumptions (A1) and (A2) can be satisfied. When they are not, the control objectives (the weight selection) should be reconsidered. On the other hand the assumptions (A3) and (A4) cause serious problems when the controlled plant P has weakly damped modes. Weakly damped modes prevent the synthesis algorithm to converge because they are interpreted by the algorithm as if they were on the imaginary axis. During the work this phenomena has been encountered for damping under approximately 0.01.

To handle this situation, it is possible to either increase the damping in the plant model or shift the augmented plant's zeros and poles away from the imaginary axis. When changing the damping, the plant uncertainty is increased and it is necessary to assure that the upper bound of uncertainty (cf. W_3 for multiplicative model) is sufficient. When shifting the poles and zeros of augmented plant away from the imaginary axis, the eigenvalues of the system matrix G are modified by a simple addition of a small multiple (e.g. $\beta = 0.01$) of the identity matrix

$$A' = A + \beta\, I.$$

Finally, when the iterative algorithm approaches the optimum, some coefficients of the controller C approach zero (or infinity). This leads to out-of-band roots of C and they should be replaced with astatic roots or removed from the transfer C.

Let us end this section with two remarks on the weighting functions. Note that the algorithm tries to cancel roots of the weights. So it is important (and natural at the same time) to approximate the weighting functions with stable filters, as it has been proposed in the 2.3. Until now one could build up the state-space model (2.13) simply by connecting the state-space models of individual systems P,W_1,W_2,W_3 and W_4. Unfortunately when high frequency roll-off is among the design objectives, the corresponding weight W_3 should be nonproper and does not have state-space model.

To handle this problem, [12] proposes an elegant remedy. Let the controlled plant P have a state-space model A_P,B_P,C_P,D_P. In case that W_3 has the form

$$W_3 = k_3\, s^2, \tag{2.14}$$

and that with this degree of W_3, the series connection of P and W_3 is proper, the control error z_3 is

$$z_3 = k_3\, \ddot{y} = k_3\, \left(C_P\, A_P^2\, X_P + C_P\, A_P\, B_P\, (d + W_4\, u)\right).$$

This observation can be generalized in order to have greater freedom when shaping the weight W_3. Consider a plant P with relative order k and filter W_3 in the form

$$W_3(s) = W_0(s)\, p(s),$$

where $W_0(s)$ is an arbitrary biproper transfer function and $p(s)$ is a polynomial with degree m. Then there exist a state-space model of the series connection $W_3\, P$ iff $m \leq k$. In Chapter 4 it will be shown that the weight

$$W_3 = \frac{k_3\, s^2}{(s/\omega_3 + 1)}$$

has given better results than the double derivator (2.14). Note that in this case the reasoning about the state-space model is particularly straightforward, because only the expression for the first derivative of y

$$\dot{y} = C\, A\, X + C\, B\, u + D\, \dot{u}$$

needs to be evaluated. Assume that the plant has a relative order at least 1, then the matrix D is zero. Moreover, this is invariant to any state-space transformations. Thus there exists a state-space representation of the series connection of the plant G and the weight W_3. However, there exists yet another remedy to this problem. Without loss of much of the closed-loop performance it is possible to add sufficient number of poles at very high frequencies to obtain a proper weight W_3.

2.5 Example

Properties of $\mathcal{H}_\infty$ synthesis can be best shown on an example. Consider a simple DC servo with transfer function from input voltage u to output velocity ω, that has been theoretically evaluated as

$$P_{model} = \frac{2.01 \cdot 33.49}{s + 33.49}$$

The output speed is measured with tachometer, so the measured velocity contains ripple noise. The tachometer's data sheet contains information that the ripple frequency is 14 cycles per turn. The input voltage applied to the servo is bounded (due to supply

voltage of the amplifiers) by ±5V. Data sheet of the motor warns against high frequency input signals and insists that frequencies beyond 50 Hz could damage the gearbox and the brushes. Finally, this DC servo is a small one, so noticeable static friction can be expected. The design objectives are following:find a reliable controller that provides precise and fast enough response of the servo and eliminates the influence of the ripple noise and possible disturbances.

The servo's dynamics have been identified from several step responses and it has been found, that as a linear approximation, the following transfer function can be used

$$P_{ident} = \frac{1.688 \cdot 19.46}{s + 19.46}.$$

The expression for P_{ident} is different from the one for P_{model}. Moreover, it depends on u as a result of the present static friction. Thus the plant model is uncertain and an upper bound for the multiplicative description of uncertainty **??** has been found to be

$$W_{3uncert} = \frac{0.743\,(s + 2.744)}{s + 19.46}.$$

The tachometer's ripple has been analyzed and it has been found that influence of the sensor noise can be bounded by a weighting filter

$$W_{3noise} = \frac{0.237\,(s + 125.7)}{s + 942.5}.$$

Requirements of precise and fast response on input command can be evaluated as follows. The request for fast response leads to high bandwidth of the closed-loop transfer T. If the closed-loop bandwidth was set too high, it could result in excessive amplitude of the input voltage u or even lead to instability of the closed-loop (due to model uncertainty). So it is wise to set the desired bandwidth to e.g. twice the bandwidth of P_{ident}.

The request for precise response can be satisfied by asymptotic tracking of step responses (type-1 control). Note that if higher order control was needed, it would be natural to use a position sensor instead of tacho. Otherwise, potential slipping would cause irreversible errors.

Attenuation of disturbances needs the sensitivity S to be small. Above all, this means minimal peaking at the crossover region. To avoid damaging the mechanical parts, closed-loop bandwidth should not exceed 50 Hz. Finally, the input voltage is limited up to ±5V. The plant alone has gain 1.688. In order not to loose much of the speed range let the input sensitivity U be bound by 1.18 dB (this value corresponds to loss of 50 % of the velocity range).

All the mentioned objectives together formulate the controller synthesis problem and should be satisfied by a controller with possibly the simplest structure, i.e. with low system order. This means that the weighting functions should have low order too. W_1, that shapes sensitivity S, should guarantee the type-1 control (i.e. have pole at zero) and should not permit larger peaking at crossover region. W_3 should guarantee the roll-off at frequencies beyond the bandwidth. −40dB/decade should be enough. This leads to

nonproper W_3 and has been remedied adding two high frequency poles to the weighting filter. W_2 shapes the input sensitivity U and should (together with W_3) guarantee that the input u of the servo would not include frequencies beyond 50 Hz. This leads to nonproper weight once again and has been handled in the same manner as W_3. There is no need to minimize the disturbance sensitivity

After some iterations the following weights have been found to best satisfy the control objectives

$$\begin{aligned} W_1 &= \frac{0.8\,(s\,+\,47.12)}{s}, \\ W_2 &= \frac{100\,(s\,+\,469)^2}{(s\,+\,5095)^2}, \\ W_3 &= \frac{1000\,(s\,+\,97.58)^2}{(s\,+\,3670)^2}. \end{aligned}$$

The resulting controller has been found for $\gamma = 1.43$

$$C = \frac{7.212e^{-5}\,(s\,+\,1859)\,(s\,+\,19.46)\,(s^2\,+\,9923s\,+\,2.516e^7)}{s\,(s\,+\,2064)\,(s\,+\,1946)\,(s\,+\,857.1)\,(s\,+\,361.7)}.$$

It is obvious that 2 of the 5 controller modes are beyond 300 Hz and can be taken away without noticeably changing the closed-loop behaviour

$$C_{red} = \frac{3.131e^5\,(s\,+\,19.46)}{s\,(s\,+\,361.7)\,(s\,+\,857.1)}.$$

Note that the compensator has canceled the pole of servo at 19.46 rad/s. This happened according to the *equalizing property* of particular type of solutions to the $\mathcal{H}_\infty$ synthesis problem [29]. The equalizing property states for the fact that the $\mathcal{H}_\infty$ synthesis "tries" to find a controller that would minimize the weighted norm in 2.4 and, moreover, assign it a constant value over all frequencies.

Figures 2.8 and 2.9 display results of the $\mathcal{H}_\infty$ synthesis. Remark that the algorithm has almost exhausted the given frequency weighted bounds. Thus the controller C_red can be thought as nearly optimal in sense of the given frequency domain specification. Further enlargements of the closed-loop bandwidth can be done only at the cost of larger input voltage amplitude and (or) higher sensitivity to disturbances. Note that the frequency domain specification has been constructed almost independently on the initial vague control objectives. This is a typical situation and usually the controller designer should make some preliminary tests and analyses of the plant to find out a feasible set of (frequency domain) specifications. However, this is often an iterative process.

2.6 Conclusions

This chapter has proposed how to formulate control objectives in a way suitable for $\mathcal{H}_\infty$ synthesis. It has pointed at important problems that are faced during the controller

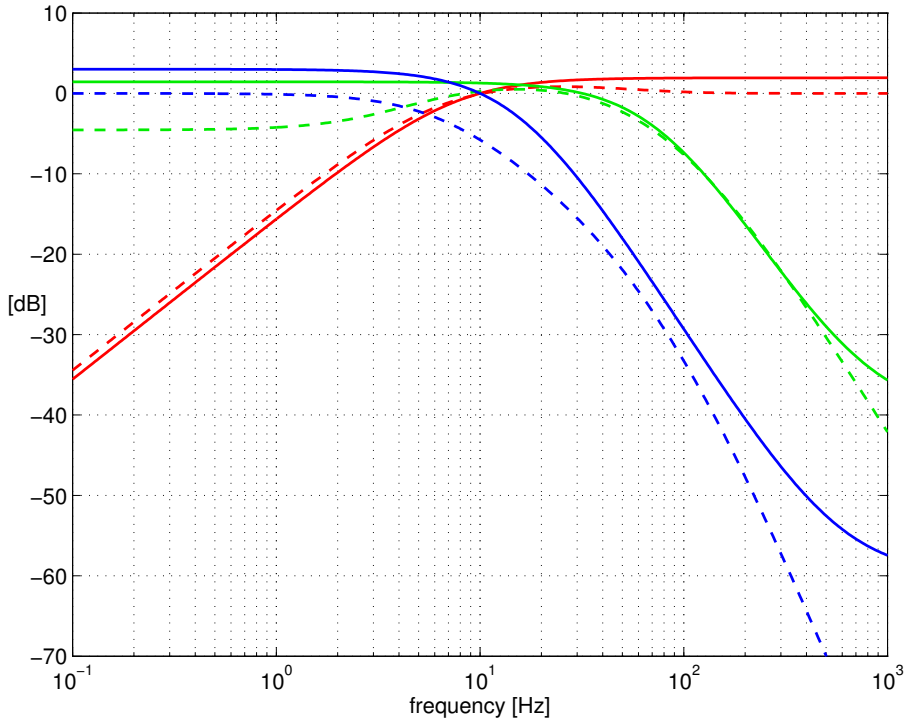

Figure 2.8: Closed-loop transfer functions and their respective bounds - sensitivity (dashed red) and $1/W_1$ (solid red), input sensitivity (dashed green) and $1/W_2$ (solid green), complementary sensitivity (dashed blue) and $1/W_3$ (solid blue)

design. These theoretical remarks will be found useful during the controller design for both VLT and Rotary Experiment. However, the next chapter is devoted to model order reduction.

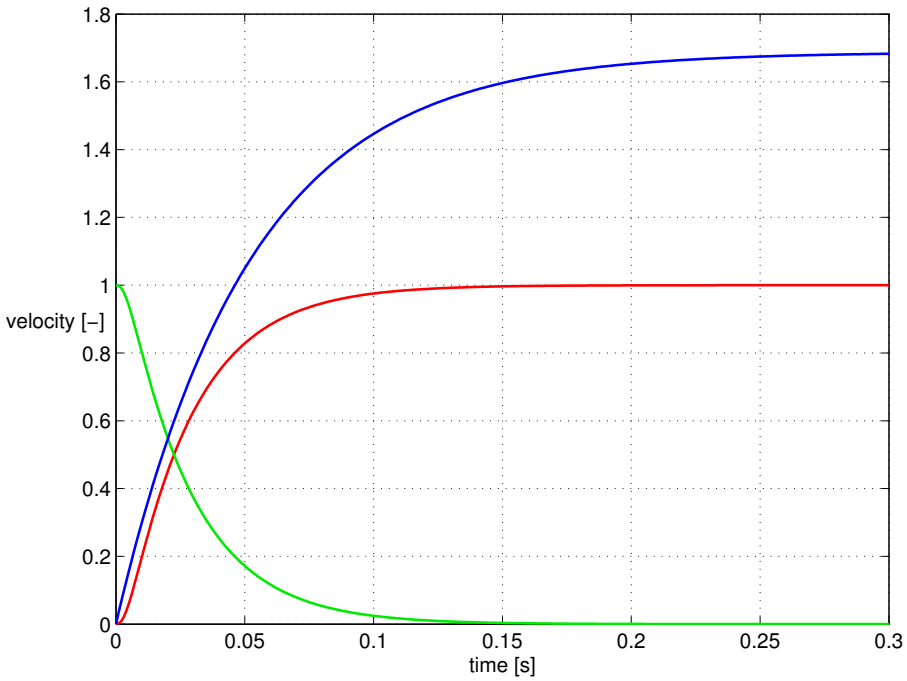

Figure 2.9: Closed loop responses on step command (red) and step disturbance (green) and response on step command of the servo alone (blue)

Chapter 3

GUI for Model Order Reduction

This chapter goes through methods for reducing the order of a plant or controller model and describes a *Graphical User Interface* (GUI) that has been implemented in Matlab to speed up the model reduction procedure and make it easy.

3.1 Introduction

Modern controller design methods such as $\mathcal{H}_\infty$ cope with higher order models of both plant and controller. When designing for optimal control, it is necessary to use the best possible plant model. Naturally, the need for precise model results in higher order plant description (e.g. FEM modelling in the field of flexible structures). The higher order models typically contain subsystems that are somehow less important than the rest. These parts of plant models can be discarded without a greater loss of accuracy. Moreover, they can cause failure of the synthesis algorithm. Hence, it is sometimes even necessary to reduce the plant's model order. Finally, $\mathcal{H}_\infty$ optimal synthesis gives controller with order equal to that of the augmented plant. Thus the model reduction can be applied on the designed controller so as to reduce its complexity while preserving the closed-loop stability and performance.

There are many model reduction techniques as the problem of simplifying the system description has been found crucial not only for $\mathcal{H}_\infty$ optimal control (e.g. statics or VLSI circuits modelling). On the other hand many of these techniques are suitable rather for larger scale models and therefore are not of interest. As this work is focused on $\mathcal{H}_\infty$ optimal control within the Matlab environment, only the methods implemented in Matlab will be taken into account. Note that these reduction techniques are based on the state-space system description and only the continous-time case is considered.

This Chapter is organized as follows. Section 3.2 introduces a measure for the aforementioned "importance" of model subsystems (i.e. grammians of observability and controllability), precisely formulates the model reduction problem and describes the actual reduction methods. Next section describes the implemented GUI and lists its capabilities.

Section 3.4 demonstrates on the VLT model how to use the GUI. At last, Section 3.5 concludes this Chapter.

3.2 Order Reduction Methods

The model reduction problem can be formulated as follows. Given a higher order LTI model G, find a lower order approximation G_r such that some norm of the difference $\|G - G_r\|$ is small. By model order, the dimension of the state vector in a minimal realization is meant (i.e. the McMillan degree) [33]. To evaluate the difference between original and reduced model, $\mathcal{H}_\infty$ and Hankel norms are used. The latter will be introduced when needed.

During the model reduction it is necessary to decide which state variables should be kept and which can be discarded. The controllability and observability grammians W_c and W_o, respectively, help to do so [34, 36]. Consider a stable system with state-space model A, B, C, D, then the grammians W_c and W_o are defined as solutions to the following Lyapunov equations [36].

$$\begin{aligned} A\,W_c + W_c\,A^* + B\,B^* &= 0 \\ A^*\,W_o + W_o\,A + C^*\,C &= 0 \end{aligned} \tag{3.1}$$

In case that the grammian is diagonal, i-th number on the diagonal of W_o reflects how the state variable x_i is observable at the output, and i-th number of W_c reflects the energy cost to control x_i. If G is stable and minimal, it is possible to find a state-space realization in which both grammians are diagonal and equal to each other

$$W_c = W_o = diag(\sigma_1, \sigma_2, \, .. \, , \sigma_n). \tag{3.2}$$

The numbers

$$\sigma_1 \geq \sigma_2 \geq \sigma \, .. \geq \sigma_n > 0$$

are called Hankel singular values.

This realization is called *balanced* and an expression for the respective transformation matrix can be found e.g. in [36, 35]. Consider the i-th state variable x_i once again. If σ_i is large, then the i-th numbers of both W_c and W_o are significant. This means that x_i can be easily controlled and has remarkable influence on the system output y. On the other hand, if σ_i is small, then it is hard to excite the i-th system mode and difficult to observe this mode at output at the same time. Hence state variables with large Hankel singular value σ should be preserved and state variables with small σ can be discarded.

Formulation of the model order reduction procedure can be given as follows. Consider a stable system G with balanced state-space realization

$$G_r = \left(\begin{array}{cc|c} A_{11} & A_{12} & B_1 \\ A_{21} & A_{22} & B_2 \\ \hline C_1 & C_2 & D \end{array}\right),$$

with $W_c = W_o = \mathrm{diag}(\Sigma_1, \Sigma_2)$ where

$$\Sigma_1 = \mathrm{diag}(\sigma_1, \sigma_2, \ldots, \sigma_k), \Sigma_2 = \mathrm{diag}(\sigma_{k+1}, \sigma_{k+2}, \ldots, \sigma_n)$$

are the diagonal submatrices of W_c and W_o corresponding to the partitioned state vector $x = (x_1, x_2)$. Then the reduced order model G_r

$$G_r = \left(\begin{array}{c|c} A_{11} & B_1 \\ \hline C_1 & D \end{array}\right), \tag{3.3}$$

obtained by truncation is asymptotically stable, minimal (and balanced) and the reduction error satisfies the bound

$$\|G - G_r\|_\infty \leq 2\,(\sigma_{k+1} + \sigma_{k+2} + \cdots + \sigma_n). \tag{3.4}$$

Except for truncation it is possible to "residualize" the states $(x_{k+1}, x_{k+2}, \ldots, x_n)$. This means simply setting $\dot{x}_2 = 0$ in the state-space equations. The reduced order model then has state-space realization [33]

$$G_r = \left(\begin{array}{c|c} A_r & B_r \\ \hline C_r & D_r \end{array}\right), \tag{3.5}$$

where

$$\begin{aligned} A_r &= A_{11} - A_{12}\,A_{22}^{-1}\,A_{21}, && (3.6)\\ B_r &= B_1 - A_{12}\,A_{22}^{-1}\,B_2, && (3.7)\\ C_r &= C_1 - C_2\,A_{22}^{-1}\,A_{21}, && (3.8)\\ D_r &= D - C_2\,A_{22}^{-1}\,B_2. && (3.9)\\ & && (3.10) \end{aligned}$$

Residualization satisfies the same error bound (3.4) as truncation. The difference between both methods is that truncation preserves the steady-state gain while residualization preserves the high frequency behaviour.

There exists an alternative to the balanced truncation. It is the so-called stochastic balancing method based on spectral factorization [33]. Consider a square stable system G with minimal realization

$$G = \left(\begin{array}{c|c} A & B \\ \hline C & D \end{array}\right), \det(D) \neq 0$$

and let W be a minimal phase left spectral factor of $G(s)\,G^T(-s)$, i.e. $W^T(s)\,W(s) = G(s)\,G^T(-s)$. A realization of $W(s)$ can be computed as

$$W(s) = \left(\begin{array}{c|c} A & B_W \\ \hline C_W & D \end{array}\right), \tag{3.11}$$

with

$$B_W = P\,C^{\mathrm{T}} + B\,D^{\mathrm{T}} \text{ and } C_W = D^{-1}\,(C - B_W^{\mathrm{T}}\,\chi)$$

where P is the reachability grammian of G and χ solves the Ricatti equation

$$A^{\mathrm{T}}\,\chi + \chi\,A + (C - B_W^{\mathrm{T}}\,\chi)^{\mathrm{T}}\,(D\,D^{\mathrm{T}})^{-1}\,(C - B_W^{\mathrm{T}}\,\chi) = 0.$$

Balanced stochastic realization of G is obtained by balancing P nad χ

$$P \;=\; \chi \;=\; \mathrm{diag}(\mu_1, \mu_2, .., \mu_n).$$

The resulting state-space realization now can be partitioned in the same way as in 3.3. Truncation of the state vector x_2 leads to a reduced order model G_r that satisfies the bound

$$\|G^{-1}\,(G - G_r)\|_\infty \;\leq\; \frac{1+\mu_i}{1-\mu_i} - 1. \tag{3.12}$$

Minimization of the approximation error norm $\|G\,-\,G_r\|_\infty$ allows to derive upper bounds on the error (viz 3.4 and 3.12). However, there exists a reduction procedure that theoretically gives even an *exact* value for approximation error [33]. This reduction method minimizes Hankel norm of the approximation error. The Hankel norm of stable system G is defined as the largest Hankel singular value (σ_1) of the system. Algorithm proposed by Glover [18] computes the balanced realization of stable G, performs a special (and tedious to describe - viz c.f. [33]) transformation of states and finally truncates the last $n - k$ states. So, except for the transformation, it is similar to classical balanced truncation. On the other hand, the Hankel norm of the resulting approximation error is exactly

$$\|G\,-\,G_r\|_\infty = \sigma_{k+1}. \tag{3.13}$$

function name	minimized norm	balancing step	input parameters
`modred`	$\mathcal{H}_\infty$	classical[1]	model order and approximation[2]
`balmr`	$\mathcal{H}_\infty$	Schur	model order, error bound
`schmr`	$\mathcal{H}_\infty$	Schur	model order, error bound
`obalreal`	$\mathcal{H}_\infty$	classical	model order
`ohklmr`	Hankel	via descriptor	model order, error bound
`ohkapp`	Hankel	via descriptor	model order, error bound
`bstschml`	$\mathcal{H}_\infty$	Schur	model order, error bound
`bstschmr`	$\mathcal{H}_\infty$	Schur	model order, error bound
`srelbal`	$\mathcal{H}_\infty$	unknown	model order

Table 3.1: List of model reduction functions

[1] computed by balreal

[2] truncation or residualization

The balancing methods introduced above try to approximate the full order model G over all frequencies. However, within many controller design problems one is only interested in a certain frequency range (see Chapter 2). This problem leads to the so-called frequency weighted balancing, i.e. finding a reduced order approximation G_r of G that minimizes the weighted error $\|W_o\,(G - G_r)\,W_i\|_\infty$, where W_i and W_o are the input and output weighting filters, respectively. This method first establishes the state-space realization for the series connection of W_i, G and W_o, then finds its ordered balanced realization and at last discards the selected states. Unfortunately, there is no known a priori error bound for the approximation error and the reduced order model G_r is not guaranteed to be stable either [36]. However, in the special case of multiplicative error minimization (set $W_i = I$ and $W_o = G^{-1}$) the reduced order model G_r is stable and minimum phase. At the same time it is possible to derive an upper bound for the approximation error

$$\|G^{-1}\,(G - G_r)\|_\infty \leq \prod_{i=k+1}^{n} (1 + 2\,\sigma_i\,\sqrt{1 + \sigma_i^2} + 2\,\sigma_i^2) - 1. \tag{3.14}$$

The methods mentioned above are implemented in Matlab (namely the Control Systems Toolbox Matlab [37], the Robust Control Toolbox [6] and the μ–Synthesis Toolbox for Matlab [2]). Note that for all the approximation methods, except for general frequency weighted balancing, it is possible to compute the error bounds a priori. This is becuase the error bounds are dependent only on the Hankel singular values σ_i corresponding to state variables x_i that are planned to be discarded. Hence the respective functions (in Matlab) offer to the designer three possible scenarios how to use them. Direct selection of the reduced order k, direct selection of the upper bound for the approximation error (the function alone finds the best order of the approximation) or plotting the system's Hankel singular values and consequent prompting for reduced order k.

Some methods have been implemented in Matlab more than once. This is partly due to the fact, that a variety of actual algorithms is related to each method ([**?**, 6, 35, 36]), partly due to coincidation of Matlab toolboxes. Table (3.1) lists Matlab functions that have been covered in the GUI.

`modred`, `obalreal`, `balmr` and `schmr` perform the model reduction based on classical grammian balancing (3.3). `modred` is the only function cappable of residualization, the other functions perform just truncation of states. `bstschml` and `bstschmr` find the stochastically balanced realization according to 3.11. The difference between `bstschml` and `bstschml` is that `bstschml` minimizes

$$\|G^{-1}\,(G - G_r)\|_\infty$$

(relative error), while `bstschmr` minimizes

$$\|(G - G_r)\,G^{-1}\|_\infty$$

(multiplicative error). `srelbal` implements the Zhou's special case of frequency weighted approximation that leads to multiplicative error minimization 3.14. Note that `bstschmr`

and `srelbal` are equivalent. `ohklmr` and `ohkapp` perform optimal Hankel minimum degree approximation 3.13. `ohklmr` uses the stabproj function to split G into stable and antistable parts and then applies `ohkapp` to each part.

All the mentioned model reduction techniques include a step when it is needed to find the balanced realization of G. This is the weakest point of the model order reduction [6, 35]. There have been many (successfull) attempts to bypass the numerically ill-conditioned balancing. The approximation functions above use either Schur method or descriptor approach [6]. A more detailed discussion of the algorithms can be found in [6, 2] and references therein.

3.3 Graphical User Interface

To provide an user-friendly interface to the mentioned approximation methods, the Order Reduction GUI has been implemented (Section 3.1). It provides the designer with a simple tool with the following key features:

1. easy access to all the functions in Chapter 3.1,
2. import/export of LTI models from/to both .mat files and workspace
3. link to LTI Viewer that enables the comparison of several reduced models with the original
4. checks against possibly incorrect method selection (stability and minimality assumptions)

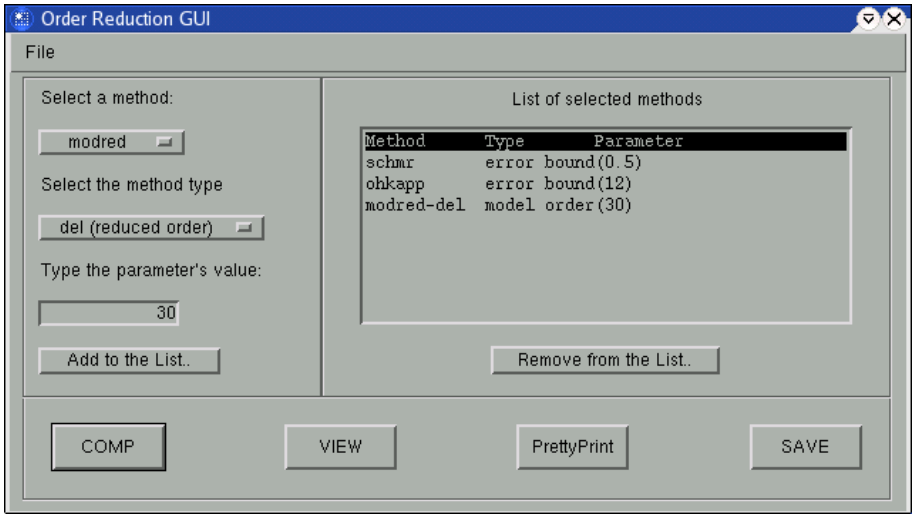

Figure 3.1: The Order Reduction GUI

The GUI is organized as follows. On the left there are two PopUpMenus, the upper one for selection of the approximation method and the lower one to select the input parameter

(according to Table 3.1). Under these PopUpMenus there is an EditBox where a value of the respective input parameter should be set. Once the approximation specification is complete, it can be added to the list of currently sheduled approximations by clicking the "Add to the List" Button. Then a new row appears in the ListBox on the right. Each row of this "MethodList" describes the corresponding setting for model reduction (approximation method, method type, input parameter value).

The bottom of the GUI contains four Buttons, COMP, VIEW, PrettyPrint and SAVE. Pressing the COMP starts the actual computation of all the scheduled approximations as they are displayed in the MethodList. VIEW opens in a new window the LTI Viewer [37] showing all the reduced models and the original full-state model simultanously. PrettyPrint displays a table of results at the propmt (model name, order and approximation method for each reduced order model). Finally, SAVE invokes the "SaveResults" Dialogue (Figure 3.2). SaveDialogue allows the user to specify the output variable names and where the output should be written. The GUI saves the original model, all the reduced models (as an LTI-array [37]) and the PrettyPrint table (character array). There is no variability in this, all the three variables will be saved.

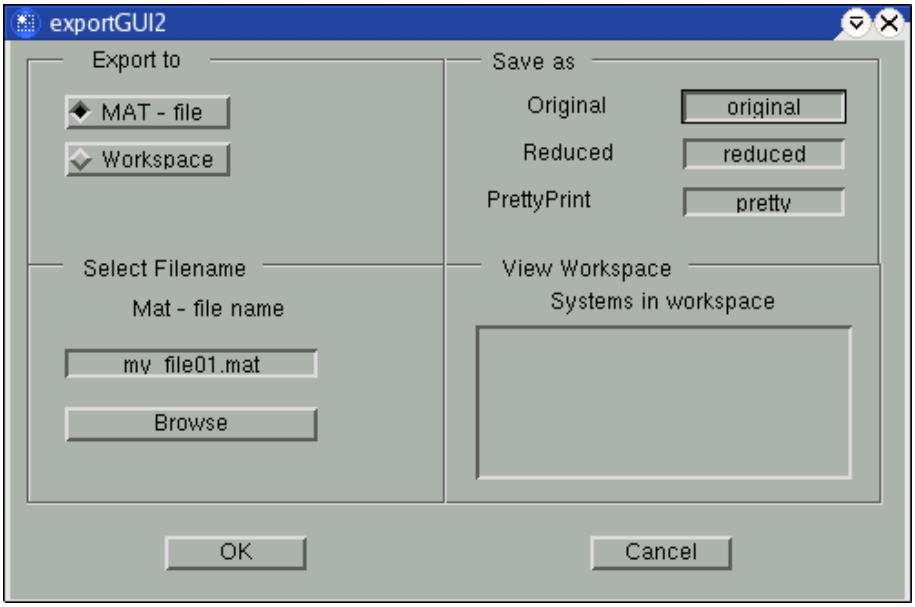

Figure 3.2: The Save Dialogue

The last feature that needs to be specified, is the import of the orioginal full-state model. This is provided by the "ImportSystem" Dialogue (Figure 3.3) which can be invoked selecting "Import.." from the FileMenu. The Dialogue displays LTI systems currently available in workspace and the designer should either select one of them or use the browser to find a .mat file to load. After selecting a .mat file, the Dialogue displays LTI systems found in the .mat file and lets the designer to choose one.

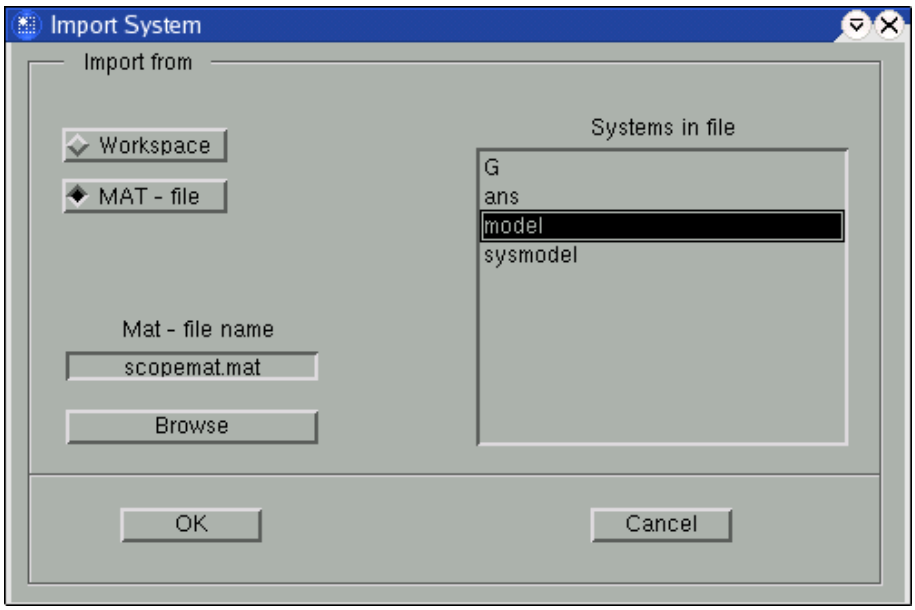

Figure 3.3: The ImportSystem Dialogue

3.4 Example

Contribution of the GUI can be best demonstrated on an example. Consider the $\mathcal{H}_\infty$ controller design for VLT. The given VLT model has 60 states. Though it is stable, it has many nearly canceled pairs of complex poles and zeros, some of them located close to the imaginary axis (nearly non-minimal). Hence it is very difficult for the state-space algorithm of $\mathcal{H}_\infty$ synthesis to even find a solution (see Chapter2). So it is wise to first find a lower order approximation of the original model and use it for a preliminary $\mathcal{H}_\infty$ synthesis. This can give an useful insight into the problem. Consequently, higher order models can be used to obtain more accurate results.

First, let us find the lower order approximation of the original VLT model. So far the approximation problem is slightly vague. Let the "lower order model" state for an arbitrary model of VLT with less than 20 state variables. The best lower order model is, according to the definition in 3.2, the one that minimizes the multiplicative error $\|(G - G_r)\,G^{-1}\|_\infty$. One method after another has been chosen and the best reduced model corresponding to each method in (3.1) has been found. The resulting lower order models are shown in (3.4) and respective multiplicative errors are shown in (3.5). 3.5 is focused only at particular frequency region important for the $\mathcal{H}_\infty$ controller design.

Note that in (3.4) there is one lower order model, called "zero-pole selection", which derivation has not been explained yet. This model was obtained simply by considering the 12 lowest poles and zeros of the original VLT model. Inspection of (3.4) and (3.5) shows that this model (dashed blue) together with the one obtained by balanced residualization (solid green) are by far the best. Above all, during the $\mathcal{H}_\infty$ design the model obtained by zero-pole selection has lead to smaller peaking of sensitivity functions S and T at the crossover region. This can be explained by the observation that it gives more accurate

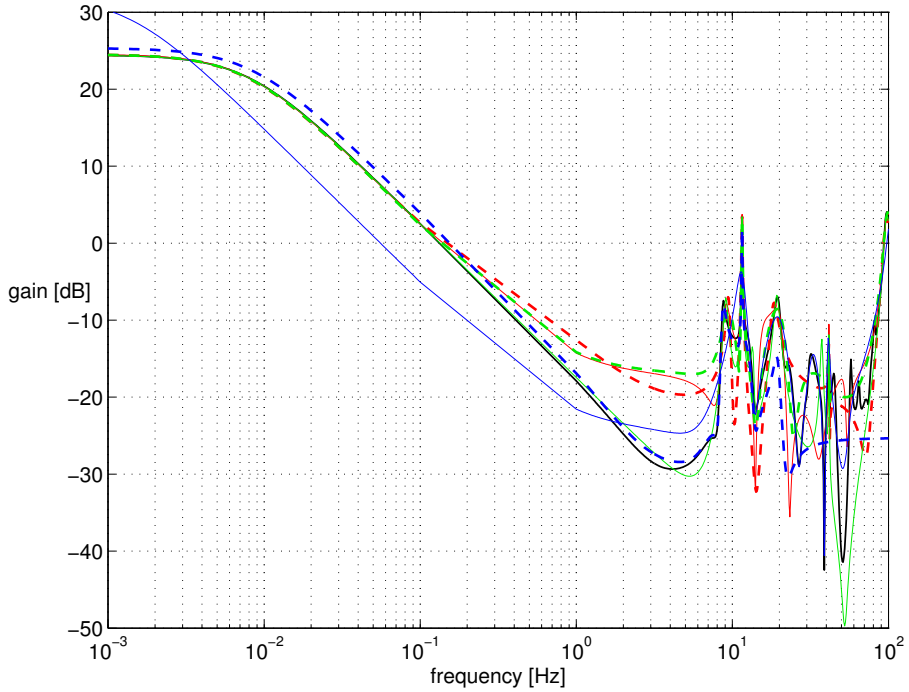

Figure 3.4: The lower order models obtained by `ohklmr` (20 states, solid red), `obalreal` (14 states, dashed red), `modred` residualization (18 states, solid green), `schmr` (18 states, dashed green), `srelbal` (18 states, solid blue), zero-pole selection (12 states, dashed blue) and the original model (solid black).

approximation of the first resonant peak than the balanced residualization.

The second task that has been stated at the beginning of this section, can be formulated as follows. Find the best approximation of the original VLT model, that will preserve as much as possible of the original behaviour and will be less ill-conditioned than the original model at the same time, i.e. the model will be free of (some) nearly canceled zero-pole pairs. To do so, one method after another has been chosen and the best reduced model corresponding to each method in (3.1) has been found. The resulting models are shown in (3.6) and respective multiplicative errors are shown in (3.7). Again, 3.7 is focused only at particular frequency region important for the $\mathcal{H}_\infty$ controller design.

Without any doubt the best approximation we have got is the stochastically balanced one (solid blue). Note that results of `bstschmr` and `srelbal` are the same. Moreover, there has been never ever found any difference between results of `schmr` and `balmr`. This is in consistence with [35], where the author says: "Matlab has built in procedures for computing balanced truncations, but these routines unfortunately do not precisely what you expect them to do.". However, the authors of the Robust Control Toolbox may be aware of some differences, so both `schmr` and `balmr` have been included in the GUI for completeness.

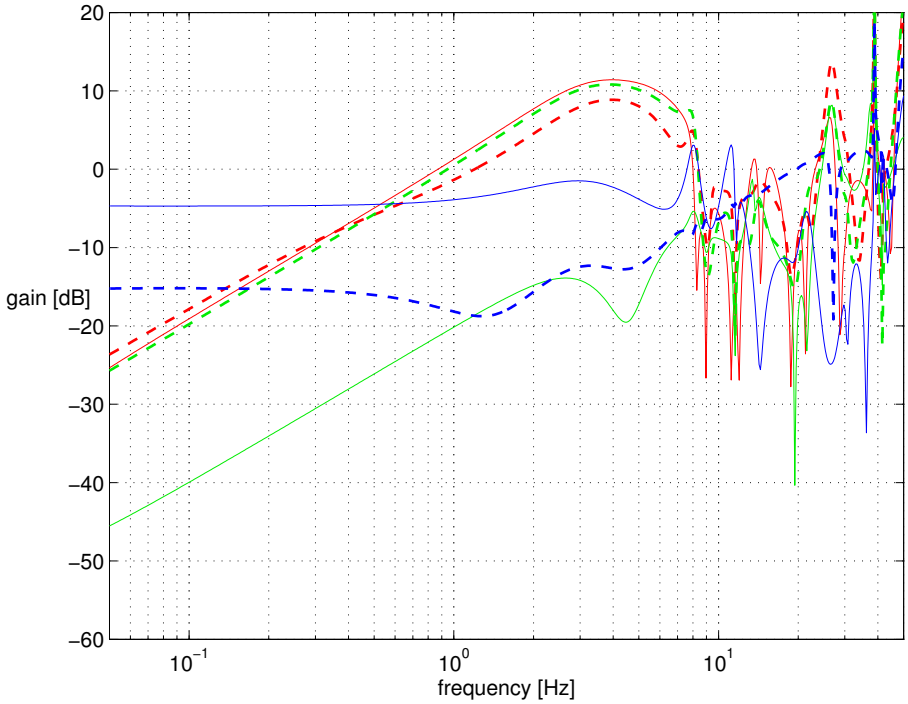

Figure 3.5: Multiplicative error of the lower order models obtained by by `ohklmr` (20 states, solid red), `obalreal` (14 states, dashed red), `modred` residualization (18 states, solid green), `schmr` (18 states, dashed green), `srelbal` (18 states, solid blue) and zero-pole selection (12 states, dashed blue).

3.5 Conclusions

This Chapter has introduced the GUI for model order reduction and has summarized approximation techniques that have been implemented within the GUI. The Order Reduction GUI speeds up the model reduction process as it offers the user quick access to various approximation methods without learning unique syntaxes of respective Matlab Toolboxes. At the same time it provides the designer with ability to immediately compare results of the individual methods.

The contribution of the GUI has been demonstrated on the VLT model. The original 60-state model is inconvenient for the $\mathcal{H}_\infty$ design. It has been arrived at the best approximation when using the stochastically balanced truncation method. Advantages of simplified models will be mentioned in the next Chapter.

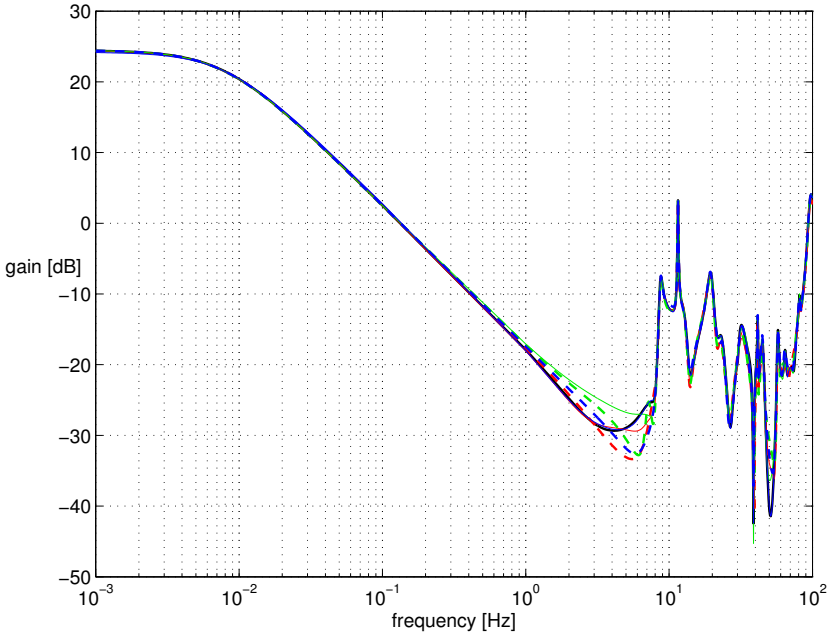

Figure 3.6: The best reduced models obtained by `modred` residualization (52 states, solid red), `modred` truncation (44 states, dashed red), `balmr` (48 states, solid green), `obalreal` (48 states, dashed green), `bstschml` (48 states, solid blue), `ohklmr` (48 states, dashed blue) and the original model (solid black).

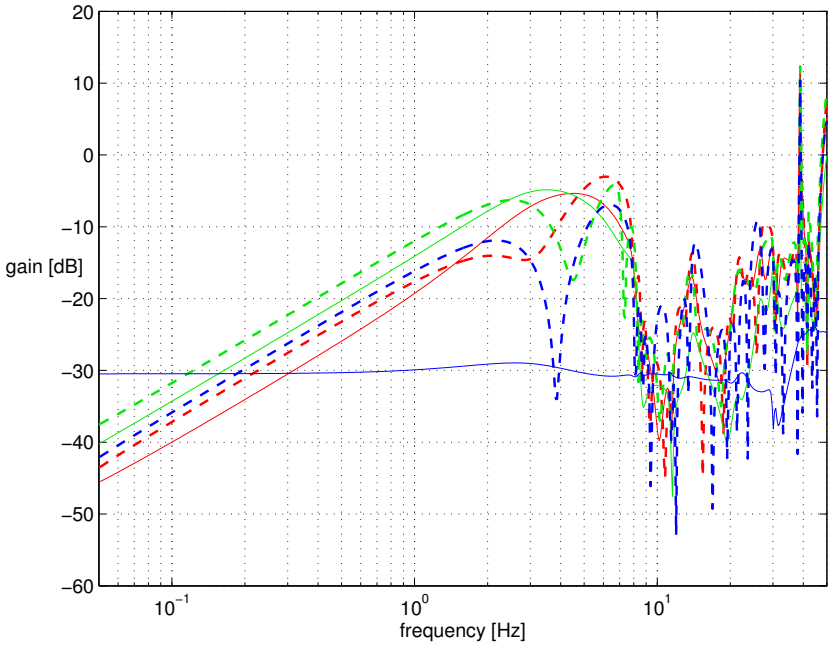

Figure 3.7: Multiplicative error of the best reduced models obtained by `modred` residualization (52 states, solid red), `modred` truncation (44 states, dashed red), `balmr` (48 states, solid green), `obalreal` (48 states, dashed green), `bstschml` (48 states, solid blue), `ohklmr` (48 states, dashed blue).

Chapter 4

Position Control of the VLT Telescope

The objective of this chapter is to design an $\mathcal{H}_\infty$ controller for the VLT telescope and compare it to the existing solution. The goal is to control position in the VLT's altitude axis. The controller should avoid the structure from vibrations and eliminate the influence of wind disturbances while preserving an acceptable response on reference commands.

Figure 4.1: VLT telescopes at Cerro Paranal

4.1 Introduction

VLT telescope is an acronym for Very Large Telescope. A set of four VLTs, known as VLT Interferometer (VLTI), is operated by the European Southern Observatory and located on Cerro Paranal, Chile (Figure 4.1). The individual telescopes are referred to by their South American Indian names, Antu, Kueyen, Melipal, and Yepun.

Each telescope possesses two-mirror optical configuration consisting of 8.2 m primary mirror and convex secondary mirror located in front of the primary mirror focus. Once operational, the VLTI will become the largest interferometric telescope of the world with an equivalent aperture of 16.4 m [13].

Because of the 8 m mirror the supporting structure of VLT is fairly huge (Figure 4.2) and the center of gravity needs to be placed exactly above the base of the mount. This is the principle behind the altitude-azimuth mounting. The tube is oriented by rotation around a vertical axis (the azimuth axis) and a horizontal axis (the altitude axis). During tracking, both axes must be rotated at variable speeds. Fortunately, the dynamical coupling between axes is negligible and they can be controlled independently.

Requirements for axes control include an extremely low reference tracking error and a good disturbance rejection. Typical references are step command and slow tracking. The most important disturbances arise from internal excitation (generated within the telescope itself) and from wind. Internal disturbances have been minimized during the mechanical design process, but the impact of the external wind disturbance needs to be attenuated by control algorithm.

Both axes already have suitable controllers for reference tracking including some disturbance rejection. However, recently there have been efforts to further reduce the pointing error caused by wind buffets. The wind mainly affects the altitude performance, because the altitude axis is exposed to a greater wind torque. The azimuth rotation is much more protected by the co-rotating enclosure and usually influence of the wind disturbance on azimuth is neglected.

Thus the goal of this chapter is to redesign the altitude controller in order to obtain better disturbance attenuation while (at least) preserving the reference tracking accuracy and swiftness. Section 4.2 introduces the altitude axis model and discusses the identification procedure which lead to it. Section 4.3 goes through the existing control algorithm. In Section 4.4 new controllers are designed using the $\mathcal{H}_\infty$ formulation. Next section shows results of this synthesis. Finally, Section 4.6 summarizes results of this chapter.

4.2 System Modelling and Identification

The VLT telescope is a fairly complex system. During the design process the altitude structure (including mounted mirrors) was modeled using the Finite Element Method with more than 100 000 elements. For the purposes of linear simulation and controller

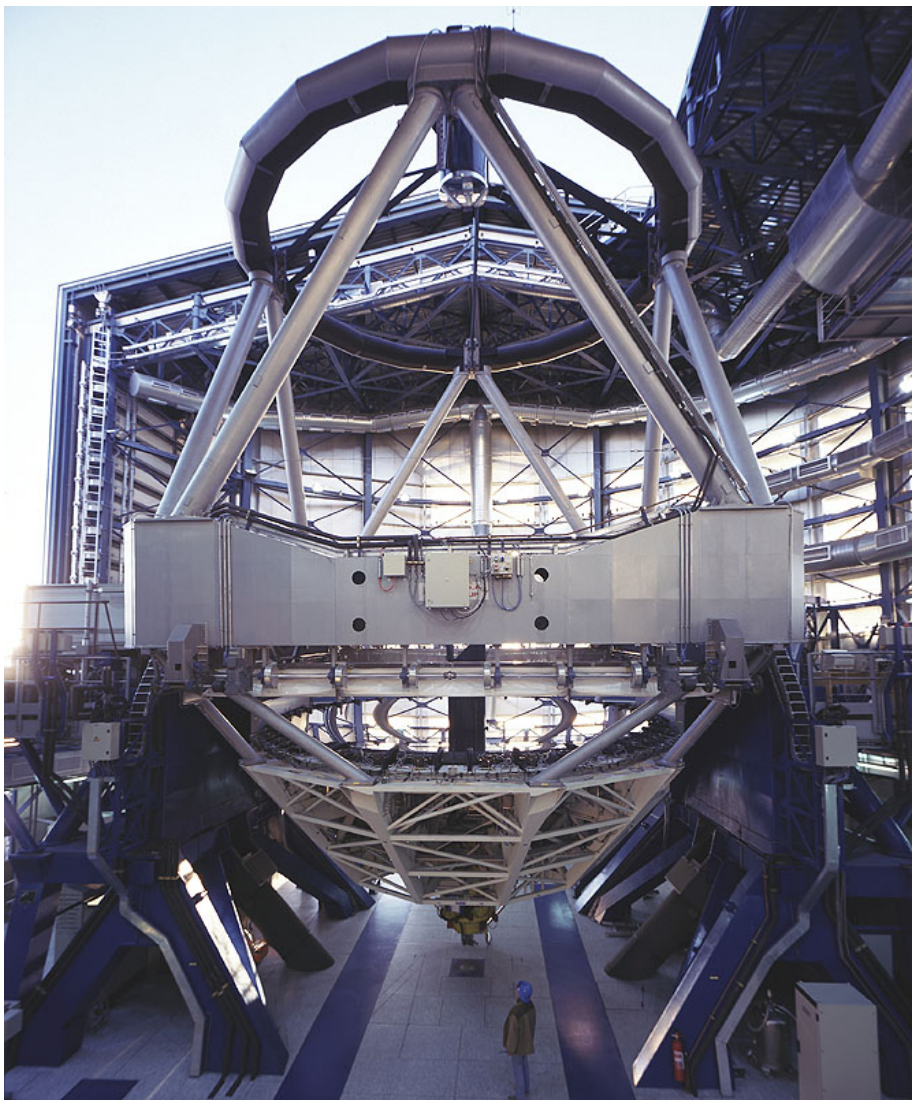

Figure 4.2: Supporting structure of VLT telescope

design the FEM model was reduced using the SMI Toolbox for Matlab [5].

However, the model used in this work was gathered the other way around (according to the correspondence with ESO engineer T. Erm). It was obtained from a time response of velocity sensors on an (not specified) input voltage applied to the altitude axes main servo. The sampling frequency was set to $f_s = 200$ Hz. The measured response was processed by System Identification Toolbox for Matlab and subsequently the order of the identified model was reduced using methods based on balanced state-space realization. This identification procedure resulted in a 60 states model (Figure 4.3).

When the system's transfer function is obtained from a response in time domain, special attention should be payed to the following problems. Sampling of the time response can give acurate results only if both aliasing and leakage are avoided (the usual ways to do so, cf. antialiasing filtering and time-domain weighting, will be discussed in Chapter 5). Figure 4.3 shows that aliasing probably was present in the measurement – notice relatively

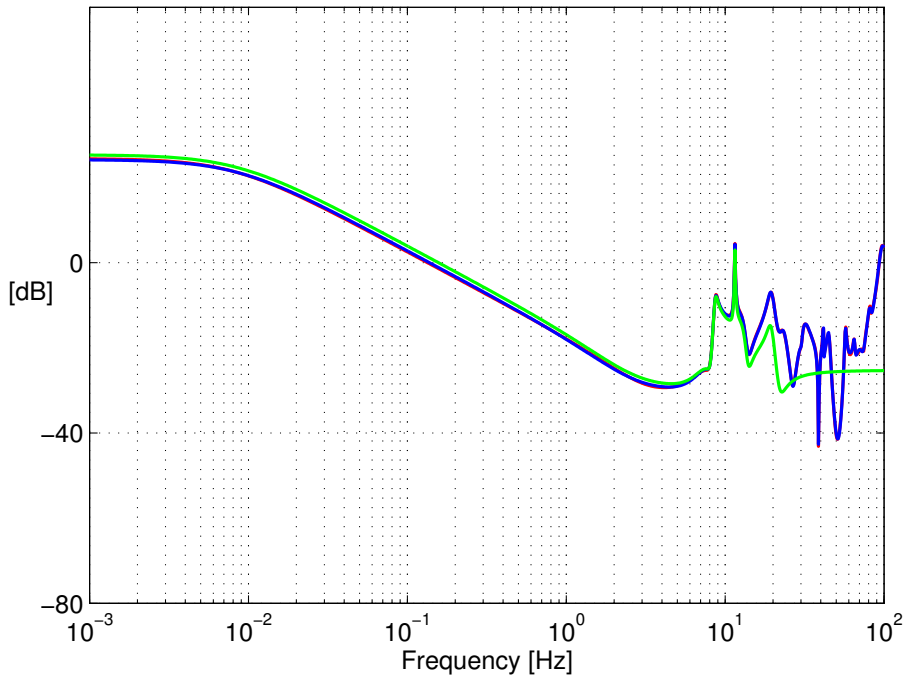

Figure 4.3: Altitude axis model - identified 60 state model (red), reduced 48 state model (blue) and reduced 12 state model (green)

high gain at the Nyquist frequency $f_N = 100$ Hz.

A crucial step of the identification is selection of the model order. Here the model order was set ad hoc, without using any prior knowledge about the behaviour of the system. In such a case one should be aware of the so-called overfitting. The overfitting occures when an identified system is fitted with a model of higher order than the true plant itself has. This happened during the identification of VLT, as can be seen in Figure 4.3. The 48 state model almost exactly matches the original 60 state model. Overfitting produces nonminimal or nearly-nonminimal paires of poles and zeros located closely together. These nearly canceled roots of the transfer function make it hard to control the plant.

Wind effects on the VLT's structure are of two sorts: static and dynamic [3]. Static wind load on the structure is given by

$$F = 0.5\, C_D\, \rho\, V^2 A, \tag{4.1}$$

where C_D is the drag coefficient, ρ is the density of air, V is the velocity of air, and A is the cross-sectional area normal to wind direction. Dynamic effects come either from the turbulence created by an obstructing surface in a flow with constant speed or from turbulence in the incoming flow itself. Airflow around individual members can generate forces normal to the wind direction due to vortex shedding. Vortex shedding can excite natural resonances in the member and result in large-amplitude oscillations at frequencies typically in the range of 1 to 100 Hz.

The turbulence content in a wind flow (wind gustiness) is characterized by the power spectral density (PSD) of the wind speed. To model the PSD of wind speed at Cerro

Paranal the von Karmán spectrum $S_V(\nu)$ was used [32]

$$S_V(\nu) = \frac{4\,I^2\,V^2\,L}{(1\,+\,70.8\,(\nu\,L/V)^2)^{5/6}}, \tag{4.2}$$

where ν is the frequency, I is the turbulence intensity in percent, V is the mean speed (in m/s), L is the outer scale of turbulence in metres, and S_V is the PSD (in m^2/s^2). The resulting PSD of the wind torque around the altitude axis is given by

$$S_\tau(\nu) = \tau^2 S_V(\nu)\,\chi_a(\nu)^2, \tag{4.3}$$

where τ is the static wind torque around altitude axis (related to the static force F from (4.1)), $S_V(\nu)$ is the wind speed power spectral density from equation (4.2), and $\chi_a(\nu)$ is the aerodynamic attenuation factor. The attenuation factor $\chi_a(\nu)$ comes from the fact that when wind acts on the VLT's structure, one must take into account the partial decorrellation of the wind speed over the telescope area facing the wind.

Inside the telescope enclosure, the incoming wind vortices are broken down into smaller ones, with size driven by the dimension of the obstruction (dome slit, louvers, etc.). This phenomena reduces amplitude of the wind buffets, but shifts wind PSD to higher frequencies which are more prone to excite the telescope structure. Thus the wind gustiness is the main source of external disturbances and for purposes of the controller design the wind torque PSD can be replaced by a second order low-pass filter with the transient frequency empirically found at approximately 1 Hz

$$PSD(s) = \frac{(2\,\pi)^2}{(s\,+\,2\,\pi)^2}.$$

4.3 Existing Controller

Controller currently used for the altitude axis tracking incorporates 2-loop PI compensator with structural filters. The inner loop is derived from a velocity sensor and takes care of the dynamics of the altitude structure, whereas the outer position loop assures pointing accuracy. The structural filters avoid the most pronounced resonant frequencies from excitation.

The controller configuration is shown in Figure 4.4. C_v, C_p and SF state for the velocity controller, the loop controller and the structural filters, respectively. Amp and c_1 are scaling factors of the altitude axis servo and position sensor, respectively. The reference command r is brought to the input of the outer position loop. The external disturbance d, caused by wind buffets, enters the system at the altitude servo output. During the identification c_1 and Amp have been included into the plant model. This should be taken into account when computing the closed-loop disturbance sensitivity function D.

The closed-loop characteristics S, T and D (defined in Chapter 2) for the altitude axis with the existing controller are shown in Figure 4.5. Note that the current setup has

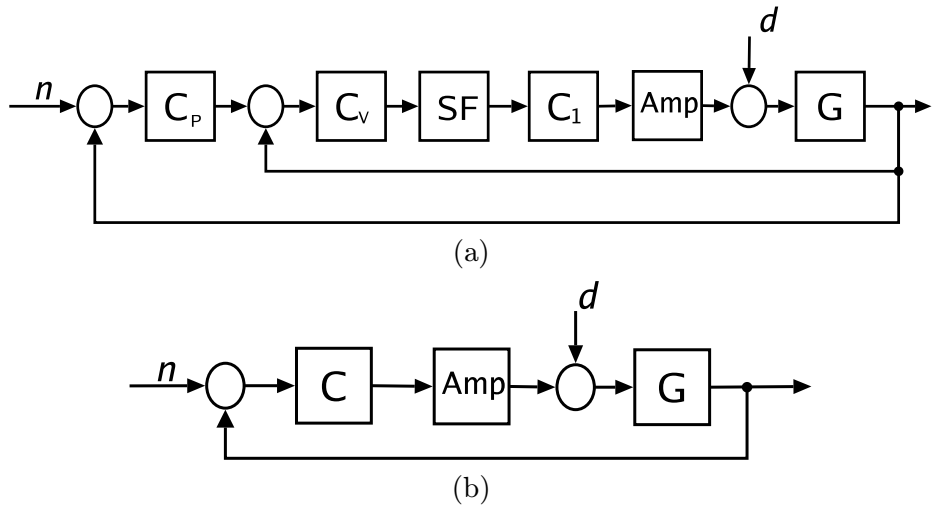

Figure 4.4: Altitude control systems - the existing 2-loop PI (a) and $\mathcal{H}_\infty$ controller (b)

been obtained after many iterations and its performance can be thought as a limit for the 2-loop PI structure. The complementary sensitivity T has a bandwidth of 2 Hz with a peak about 2.5 dB. Sensitivity function S exhibits a 6 dB peak. These results can be regarded as particularly satisfying for such a resonant system.

On the other hand the disturbance sensitivity function D exhibits an increase of magnitude approximately in the range from 0.01 Hz to 7 Hz. In this frequency interval the wind disturbances affect the altitude axis and it is desired to further diminish the disturbance sensitivity D of the output position. Improvements in D should not be done at the cost of swiftness or smoothness of the system's time response. The step response of the existing closed-loop system has a 20 % overshoot and a settling time under 1.5 s (Figure 4.10). Also the sensitivity to measurement noise (T) should be kept as low as possible. Thus the requirements on the closed-loop system can be summarized as

> diminish the disturbance sensitivity D at frequencies below approximately 7 Hz, while at least preserving the following: asymptotic tracking of constant references, low sensitivity to measurement noise, step response overshoot about 20 %, settling time under 1.5 s.

4.4 Controller Design

As the control goals have been defined and the plant has been indetified, it is possible now to design the controller. To do so, the state-space algorithm of $\mathcal{H}_\infty$ synthesis (discussed in Chapter 2) will be used.

The controller is assumed in the form shown in Figure 4.4b. Within this configuration

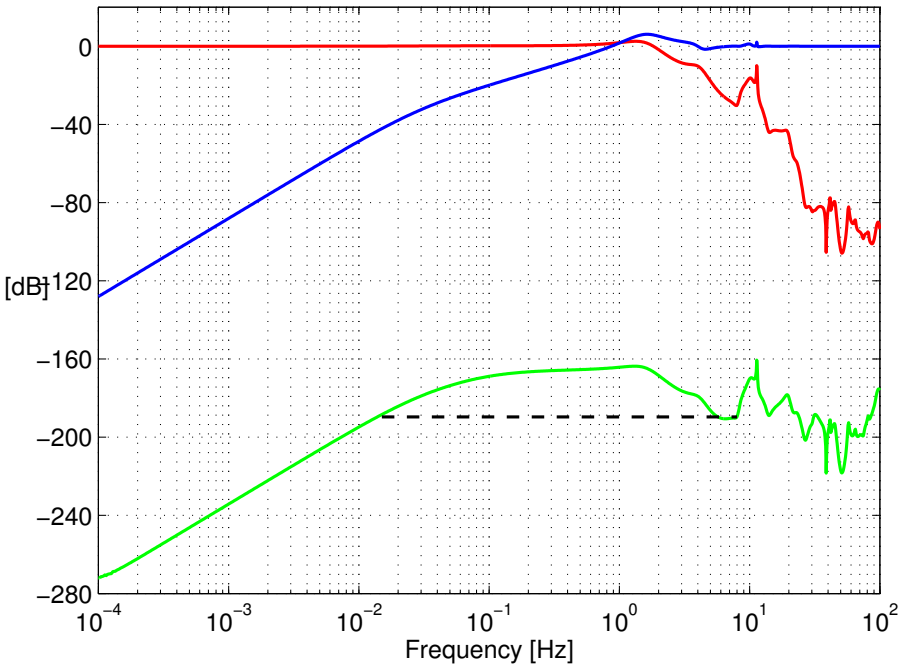

Figure 4.5: The closed-loop characteristics of the existing configuration - sensitivity S(red), complementary sensitivity T(blue) and disturbance sensitivity D(green)

the closed-loop functions S, T, U and D have the form

$$\begin{aligned} S &= \frac{1}{1+P\,C} \\ T &= \frac{P\,C}{1+P\,C} \\ U &= \frac{C\,Amp\,c_1}{1+P\,C} \\ D &= \frac{P/(Amp\,c_1)}{1+P\,C}. \end{aligned} \tag{4.4}$$

Note that within the configuration of Figure 4.4b the complementary sensitivity T has only the meaning of output sensitivity to measurement noise. Transfer function from reference r to output y (which determines shape of the closed-loop system's step response) is now

$$Tr = \frac{C_r\,C\,P}{1\,+\,C\,P} = C_r\,T, \tag{4.5}$$

Our task is to find a stabilizing controller that simultanously minimizes the magnitude of D at low frequencies (approximately below 7 Hz) and peaking of T and S at the crossover region. The responsibility for shaping T_r has been lifted from the controller C and is undertaken by the feedforward filter C_r. Thus the problem of finding suitable controller is divided into two steps. At first, stabilizing C that best fits the requirements on D, S and T will be found using the state-space algorithm of $\mathcal{H}_\infty$ synthesis. Next, C_r will be added to satisfy the demands set on T_r.

To find the compensator C, approach formulated in Chapter 2 is followed. A stabilizing C that minimizes the $\mathcal{H}_\infty$ norm

$$\min_C \mathcal{H}_\infty = \min_C \left\| \begin{pmatrix} W_1\,S & -W_1\,D\,W_4 \\ W_2\,U & -W_2\,T\,W_4 \\ W_3\,T & W_3\,D\,W_4 \end{pmatrix} \right\|_\infty \tag{4.6}$$

is looked for. Shape of weighting filters is derived from requirements on the closed-loop system and from properties of the controlled plant. The weighting filters should have simple form in order to avoid numerical conditioning problems of the synthesis algorithm.

The highest possible attenuation of wind disturbances is called for. Thus the disturbance sensitivity D should be minimized at frequencies approximately below 1 Hz. On the other hand there is no need in attenuating D at high frequencies, as the wind torque PSD is negligible there. W_4 can be chosen in the form

$$W_4 = \frac{k_4\,\omega_4^2}{s^3 + 2\,\xi_4\,\omega_4\;s^2 + \omega_4^2\,s}.$$

At low frequencies W_4 behaves like simple integrator. Introduction of the complex pair of poles allows advanced shaping of W_4 in the crossover region.

The requirement of constant reference tracking implies that the sensitivity function S should have zero at 0. This is already ensured by the choice of W_4 and by the fact that the plant P has an astatic pole. In the crossover region peaking of S should be minimized. This can be done considering the weights

$$\begin{aligned} W_{1a} &= k_1\,\omega_1 s + \omega_1, \\ W_{1b} &= \frac{k_1\,\omega_1\,(s+\omega_1)}{s}. \end{aligned}$$

At low frequencies W_{1a} and W_{1b} have the same gain. The only difference between W_{1a} and W_{1b} is that the state-space model of W_{1b} has nonzero matrix D. Sometimes this can help the algorithm to give better results.

The closed loop transfer function T is desired to have a high bandwidth so as to fast step response of the closed-loop system can be established. Although T_r will be shaped by the prefilter C_r, significant improvement of the shape of T could be done only at the cost of overly large control input u. On the other hand, stability and performance robustness to plant uncertainty require small T, especially at high frequencies. Inspection of the controlled plant shows that P has a RHP zero at 6 Hz and lowest pronounced resonant frequency at 8 Hz. According to Freudenberg-Looze equality (2.9), bandwidth above 6 Hz would be reached at the cost of excessive peaking of both S and T. Transient frequencies ω_1 and ω_3 of the weights W_1 and W_3 should not exceed this bound. Consider the following two forms of W_3

$$\begin{aligned} W_{3a} &= k_3\,s^2, \\ W_{3b} &= \frac{k_3\,s^2}{s+\omega_3}. \end{aligned}$$

Observe that the relative order of the plant P is only 1 and series connection of W_{3a} and P is not proper. The state-space algorithm cannot cope with such a configuration. But there is a simple remedy. The slowest pole of P at 0.0016 Hz can be shifted to 0 Hz. This does not influence the key frequency range and results in a new plant P_{temp} with relative order 2. Then series connection of W_3a and P_{temp} is proper and the whole augmented plant is feasible. The controller C, synthesized via the state-space algorithm, has pole at 0.0016 Hz which can be shifted back to 0 Hz.

There are no direct limitations imposed on the input sensitivity U. Though the weight W_2 is introduced into the augmented plant to improve numerical performance of the $\mathcal{H}_\infty$ synthesis algorithm. W_2 in the form

$$W_2 = k_2,$$

is sufficient.

The weighting gains k_1, k_2, k_3 and k_4 have not been selected yet. Also the frequencies ω_1 and ω_3 have only vague upper bound. Together these six parameters need to be optimized to match the control objectives as much as possible. Table 4.1 shows values of the respective parameters that have been found (after many iterations) to give the best performance. Two controllers, C_a and C_b, have been synthesized. The former with weights W_{1a} and W_{3a}, the latter with weights W_{1b} and W_{3b}.

	k_1	ω_1	k_2	k_3	ω_3	k_4	ω_4	ξ_4
C_a	16	2.3	1	1050	–	100	0.25	8
C_b	3	10	10^{-4}	10^{-2}	10	100	0.35	6

Table 4.1: Selected parameters of the weighting filters

During the iterative search for optimal controller C_a it has been observed that it is necessary to reduce order of the plant G. When using the original nonminimal model, the synthesis algorithm often fails. With the balanced 48 state model, that almost exactly matches the identified transfer function, poor results are obtained. Reduced order model, that works best within the algorithm, is a 12 state model (Figure 4.3). To get this model, the balanced 48 state model has been chosen as a starting point. Consequently, only 12 lowest poles and zeros have been considered and the rest has been taken away. In the key frequency range, the crossover region (viz Chapter 2), the 12 state model fits the identified transfer function better than any other reduced order model. Even the use of more sophisticated frequency weighted reduction techniques has not beaten this model (as it is described in Chapter 3).

After the design of closed-loop compensators C_a and C_b, prefilters C_{ra} and C_{rb} have been found. The prefilters are needed to shape the transfer function T_a and T_b in order to speed up and smooth the step responses of the closed-loop systems. To do so, the respective closed loop transfer functions have been inverted, their inversions have been simplified via `modred` reduction technique (described in Chapter 3) and multiplied by a

low pass filter with bandwidth set to 6 Hz

$$\begin{aligned} C_{ra} &= F\,T_{\text{ainv}}, \\ C_{rb} &= F\,T_{\text{binv}}, \end{aligned}$$

where

$$F = \frac{2\,\pi\,6}{s\,+\,2\,\pi\,6}$$

is the low pass filter and T_{ainv} and T_{binv} are stable approximations of T_a^{-1} and T_b^{-1}, respectively. T_{ainv} and T_{binv} cancel peaks of T_a and T_b in the crossover region and the low pass filter attenuates high frequency oscillations of the step response.

4.5 Results

The design procedure described in the previous section has lead to compensators C_a and C_b and prefilters C_{ra} and C_{rb}. These 'compensator-prefilter' pairs correspond to the weight selection given in Table 4.1. In this section, performance of both solutions is shown and compared to the existing 2-loop PI controller and a 1-DOF controller designed to minimize the classical sensitivity S. In what follows, the existing controller is marked C_{PI} and the controller designed to minimize S is marked C_S. Note that C_S has been designed only for benchmark purposes, that is, without thorough tuning of the weights.

Figures 4.6, 4.7 and 4.8 show the closed-loop disturbance sensitivity D, sensitivity S and the closed-loop transfer T, respectively.

Inspecting the results, it is clear that disturbance attenuation improvement is possible. The system has been made less sensitive to wind disturbances in the key range below 2 Hz. Simultanously, sensitivity functions have been attenuated in the same frequency region. This is of no surprise, as S and D are bound together by the relation $D = P\,S$. Above 2 Hz, the disturbance sensitivity functions more or less copy the original D_{PI}. What is the trade-off?

The sensitivity functions and the closed-loop transfers exhibit peaking of magnitude in the cross-over region and in the high frequency range . The maxima of S_a and S_b have been increased from the original value of 6.1 dB to 7.4 dB and 7.5 dB, respectively. However, this makes sense. It is desired to minimize effects of disturbances using the output measurements. This is possible only when output sensors are not disturbed by a too strong noise. Note that lower sensor noise is required only beyond 0.5 Hz, although the improvement of D is situated below 2 Hz. The attenuation of D brings down S in the low frequency range and, according to the Bode sensitivity integral and the algebraic constraint on S and T (see Chapter 2), this leads to increase of T at high frequency region. This trade-off is inevitable. Designer can only choose between high peaking of T at the crossover region and slower roll-off at high frequencies.

Peaking of the T_r has been lowered using prefilters. Though very simple, the prefilters

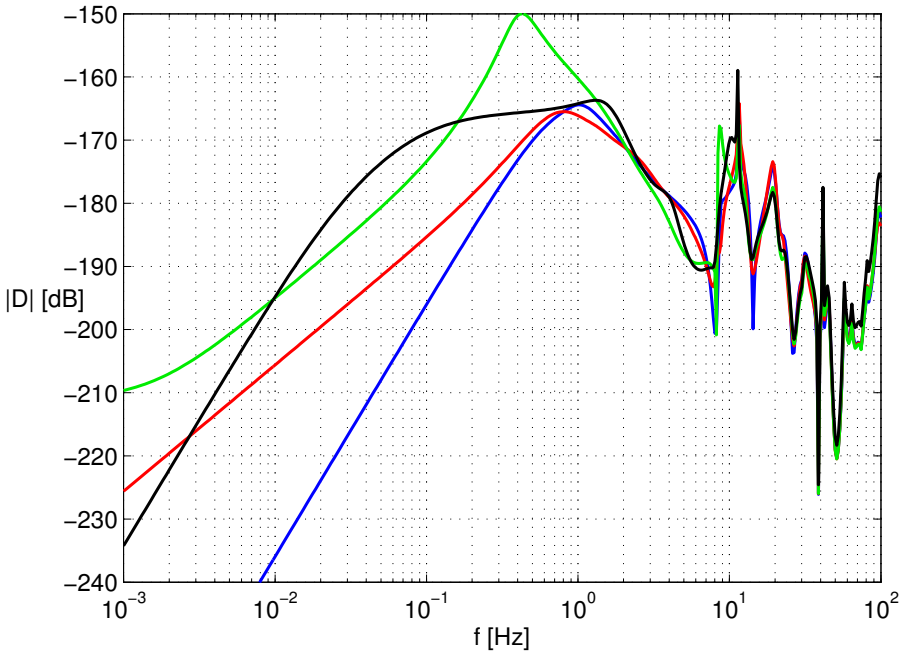

Figure 4.6: Disturbance sensitivity D of the closed-loop system with controller C_a(red), C_b(blue), C_S(green) and existing solution C_{PI}(black)

C_a and C_b (see Figure 4.9) have lead to good results in the time domain (see Figure 4.10). Closed-loop system with C_b even beats the existing solution.

When comparing the pair C_a - C_{ra} to the pair C_b - C_{rb}, it can be seen, that slightly more complicated shape of weighting filters has given better results. Namely, the disturbance sensitivity D is further attenuated, the step response is faster and has smaller overshoot and control input u_b has smaller amplitude than u_a. Another remarkable property of the solution with C_a is, that difference between the full-order and the 12-state reduced-order model leads to higher peaking of S at the high frequency range.

Comparison with the 1-DOF controller C_S brings to the following observation. Only few attempts with weights have been performed, hence the poor results of D_S have been expected. To cure this, either more sofisticated weighting filter W_1 should be used (the plant dynamics should appear in W_1 when indirectly shaping D via S), or D should be shaped directly via W_4. The latter option leads to simpler weighting filters, that are easier to shape, and should be preffered.

4.6 Conclusions

The VLT control problem has been precisely specified. It has been shown that requested wind disturbance attenuation is important at the low frequency region (approximately below 1 Hz). Two controllers, that further attenuate the effects of wind buffets, have been

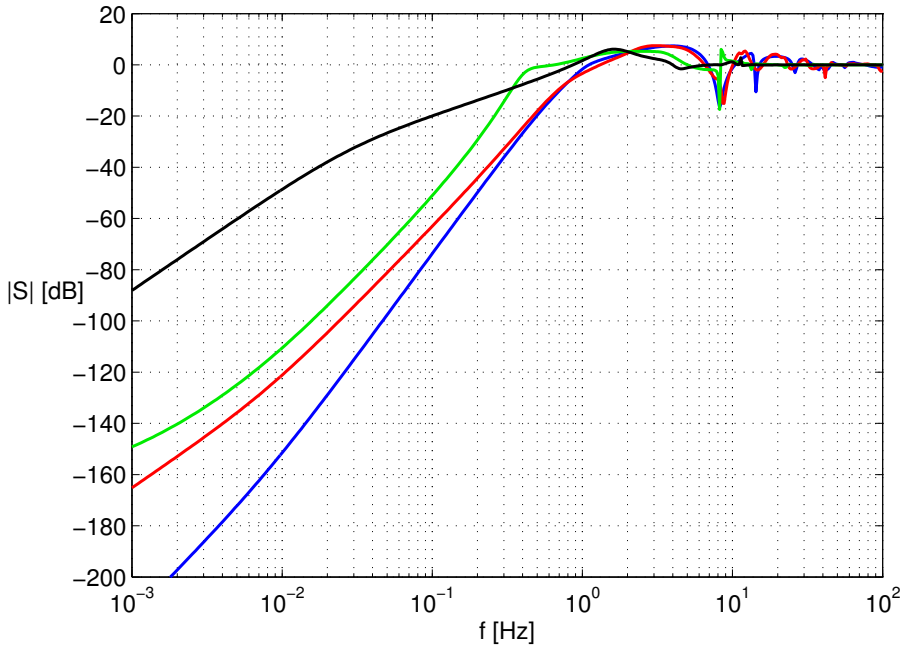

Figure 4.7: Sensitivity S of the closed-loop system with the controllers C_a(red), C_b(blue), C_S(green) and existing solution C_{PI}(black)

designed. Obtained results have lead to conclusion that this deteriorates other closed-loop benchmarks at the same time. The plant model has nonminimal zero at the crossover region. This makes the trade-off even more severe. It has been pointed out that the given plant model was possibly overfitted and thus this phenomeon could be less pronounced in the real situation.

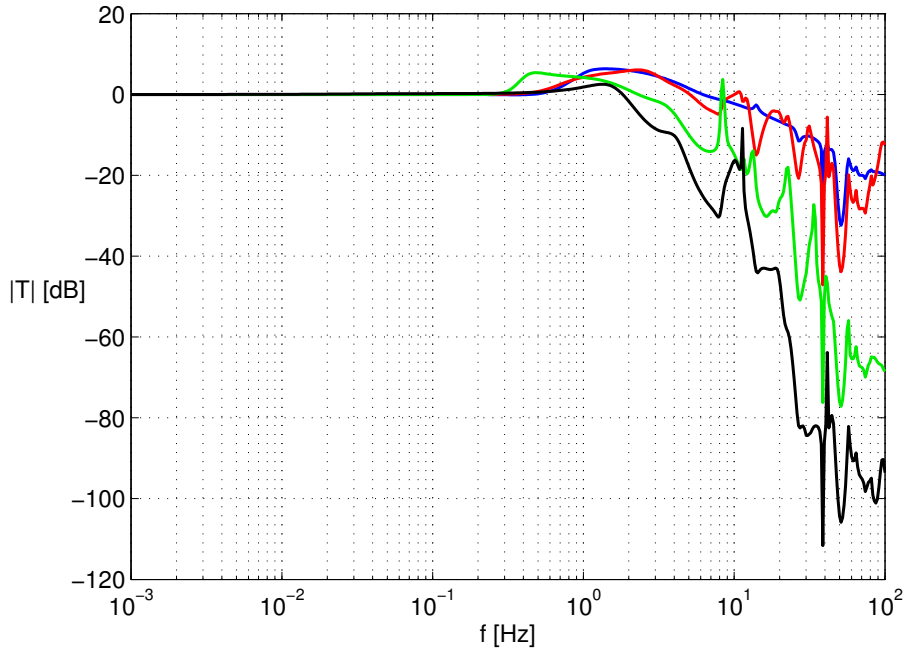

Figure 4.8: Transfer function T of the closed-loop system with the controllers C_a(red), C_b(blue), C_S(green) and existing solution C_{PI}(black)

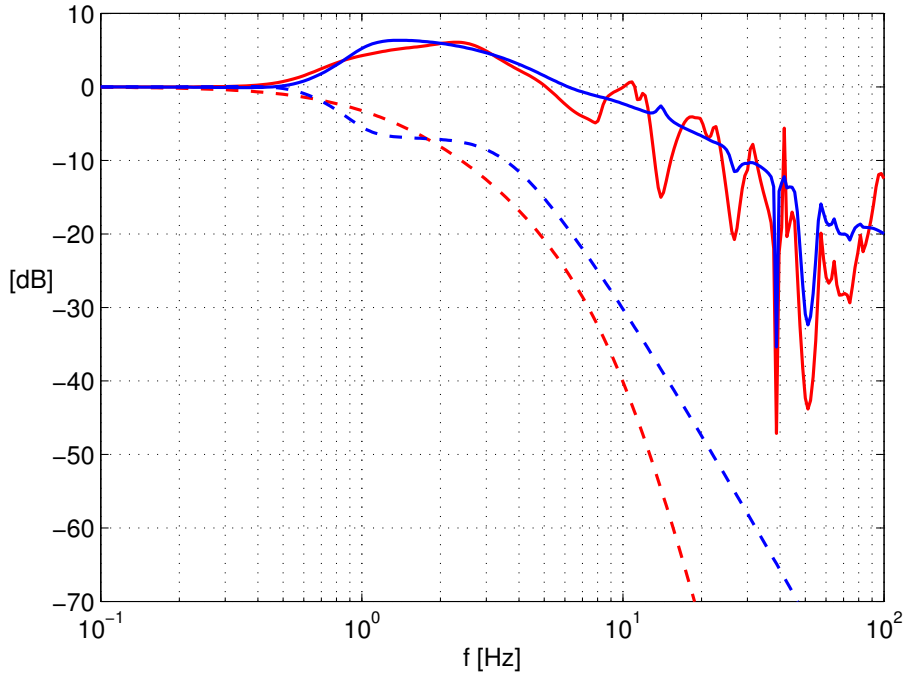

Figure 4.9: Closed-loop transfer functions T_a(solid red) and T_b(solid blue) and prefilters C_{ra}(dashed red) and C_{rb}(dashed blue)

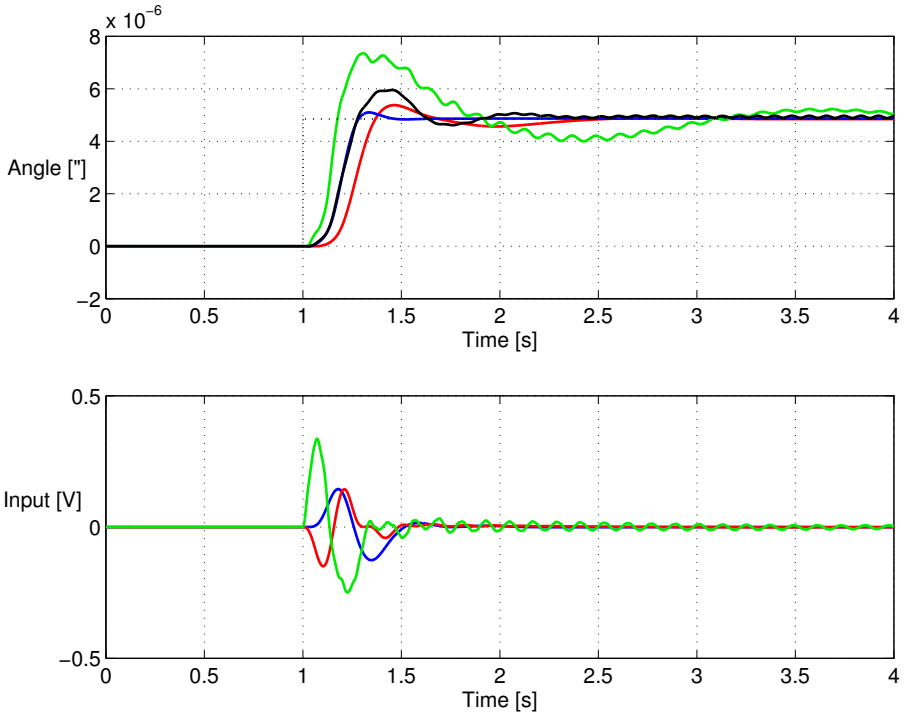

Figure 4.10: Step responses of the closed-loop systems T_a(red), T_b(blue), T_{ZH}(green) and existing solution T_{PI}(black)

Chapter 5

Rotary Experiment

The objective of this chapter is to design and test an $\mathcal{H}_\infty$ controller for the Quanser Rotary Flexible Link Experiment [30]. The goal is to control tip position of a flexible link attached to a DC servo. The controller should eliminate the link's vibrations while maintaining a fast response.

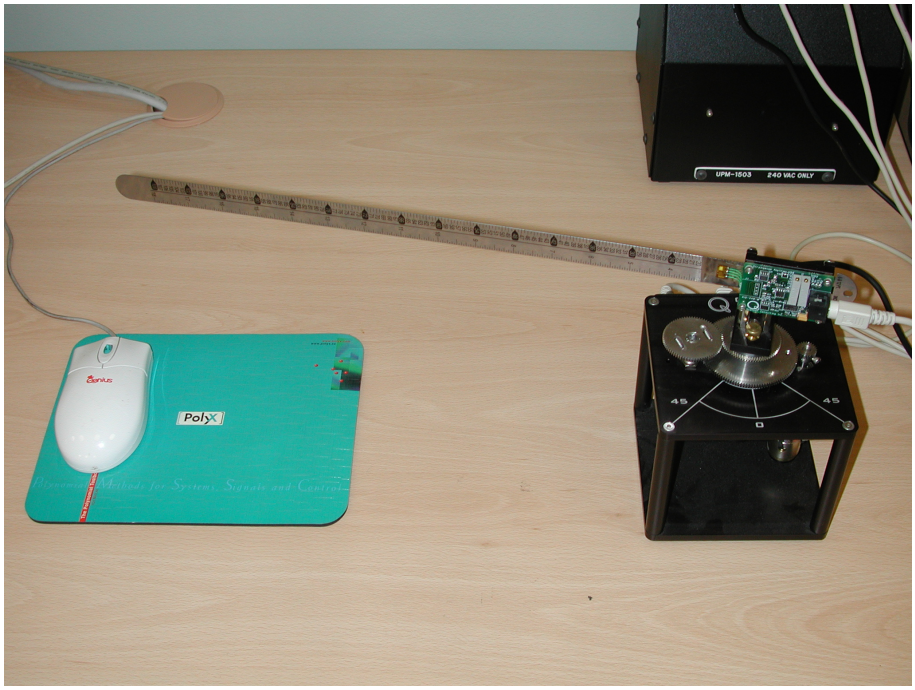

Figure 5.1: Quanser Rotary Experiment

5.1 Introduction

As stated above, the plant consists of a DC servo and a flexible link attached to the motor's shaft. The servo is voltage driven Quanser SRV02-ET model equipped with angular speed and position sensors. The flexible link is Quanser FLEXGAGE thin aluminium beam with strain gage mounted at its base. Interaction with the controled plant is provided by Quanser UPM 2405/1503 power module and by Quanser MultiQ PCI card, as shown in 5.2. Quanser supports its laboratory system with WinCon software that allows communication with Simulink. Thus the controller can be realized using Matlab.

The plant modelling is divided into three parts. In Section 5.2, model of the DC servo with gear is briefly recapitulated. Then model of the flexible link based on Hamilton's principle and Euler-Bernoulli assumptions is derived. Consequently, the mutual servo-beam interaction is introduced to the model. Having the plant satisfactorily identified, 5.4 is devoted to the controler design. Experimental results are shown and discussed. At last, 5.5 summarizes results of this chapter.

5.2 Servo Modelling and Identification

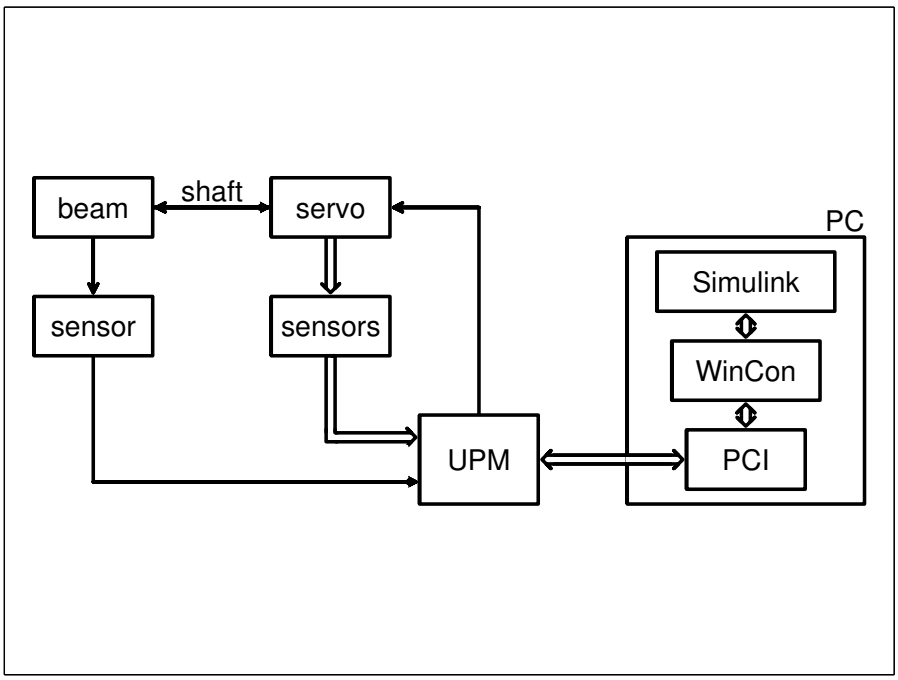

Figure 5.2: Experimental setup

The Quanser SRV02 used in the Rotary Experiment consists of a DC servo in a solid frame. The motor is equipped with a gear box. The gearbox output drives external gears.

The unit is equipped with tachometer, potentiometer and optical encoder to measure the output angular speed and position.

The servo model consists of electrical and mechanical component. The former converts input voltage to electromotiveforce (emf), the latter converts emf to output velocity and moment, see 5.3a. To derive the model, consider the electrical component of the motor first

$$\begin{aligned} u &= R\,i + L\,\dot{i} + E_{emf}, \\ E_{emf} &= k\,i. \end{aligned} \tag{5.1}$$

where u is the input voltage, R and L are resistance and inductance of the armature circuit and E_{emf} is the voltage induced due to emf (E_{emf} is proportional to armature current i).

The mechanical moment τ_m on the motor shaft, which is proportional to the armature current i, must be balanced by the other moments acting on the shaft

$$\tau_m = \eta_m\,k\,i = J_{eq}\,\dot{\omega}_m + \tau_{fricteq} + \tau_{exteq}, \tag{5.2}$$

where J_{eq} is total moment of inertia of bodies attached to the shaft, $\tau_{fricteq}$ is total moment of friction forces and τ_{exteq} is moment of load not accounted for in the two former components. Note that all moments comming from the output of the gear are considered in the equivalent form (*as seen by the motor*).

SRV02 incorporates a MicroMo Coreless DC Motor. This model is a high efficiency low inductance motor. Thus the motor inductance can be disregard and combining (5.1) with (5.2) yields

$$\tau_m = \frac{\eta_m\,k}{R}\,u - \frac{\eta_m\,k^2}{R}\,\omega_m. \tag{5.3}$$

The gear is passive two-port that transmits power with efficiency η_g while the output angular speed is n-times higher (n is called *gear-ratio*)

$$\begin{aligned} \eta_g\,\tau_m\,\omega_m &= \tau_l\,\omega_l, \\ \omega_m &= n\,\omega_l. \end{aligned} \tag{5.4}$$

Using the result (5.3) the transfer function from input voltage u to gear output angular speed ω_l has been obtained in the form

$$\frac{\Omega_l(s)}{U(s)} = \frac{K_{tacho}\,\eta_g\,\eta_m\,k\,n}{R\,J\,s + n^2\,\eta_g\,(\eta_m\,k^2 + R\,B_{eq})}, \tag{5.5}$$

where K_{tacho} is tachometer sensitivity, $J = J_l + \eta_g\,n^2\,J_m$ is equivalent inertia as seen from the load side of the gear, J_l is load inertia and J_m is motor inertia, $B = n^2\,\eta_g\,B_{eq}$ is coeficient of viscous friction that is the only admissible type of friction for LTI model

$$\tau_{friction} = B\,\omega_l = B_{eq}\,\omega_m.$$

State space model is shown in 5.3b.

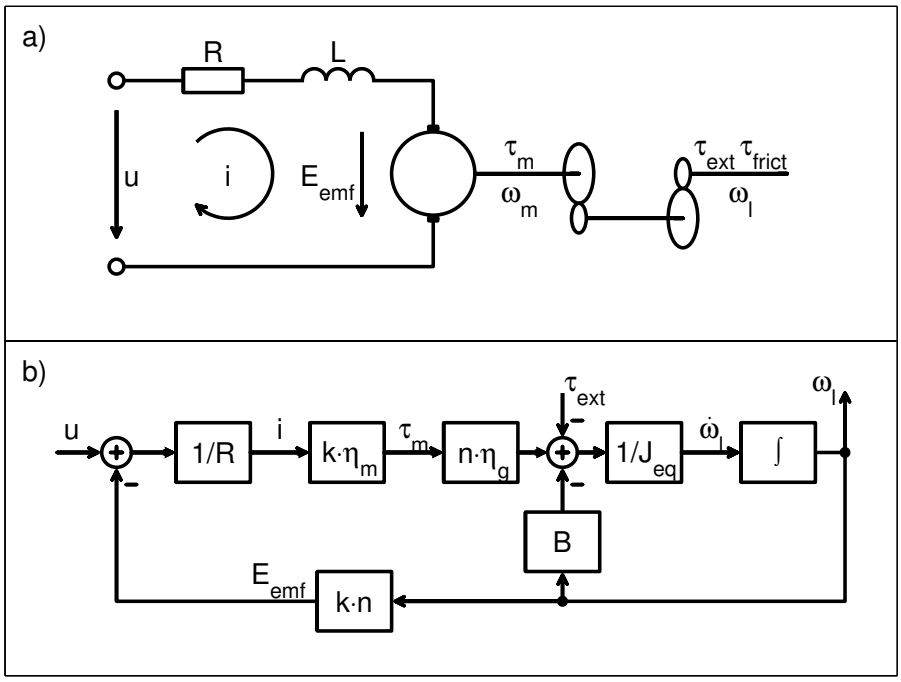

Figure 5.3: DC servo - physical setup (a) and state-space model (b)

Substitution of system parameters (given in 5.1) into the transfer function (5.5) results in the model

$$\frac{\Omega_l(s)}{U(s)} = 2.01\,\frac{5.33 \cdot 2\,\pi}{s + 5.33 \cdot 2\,\pi}. \tag{5.6}$$

To evaluate the theoreticaly calculated model, step responses of both model and physical plant (sampled with $f_s = 1\text{kHz}$) have been compared in 5.4. Inspecting the figure, two important observations can be done. The model (5.2) is rather poor estimate of the real plant and the output signal suffers from strong noise. In what follows both problems are discussed.

Since the system has very simple structure

$$G = \frac{k}{\tau\, s + 1},$$

it can be identified directly from the step response. K can be found as a steady state amplification and τ can be approximated as a slope of the step response between approximately 20 % and 80 % of its steady state amplitude [22] in the sense of mean squares [19].

Deviation of the theoreticaly obtained model comes from several origins/reasons. Influence of the parameters variation is obvious (c.f. Table 5.1). Partially the model error comes from the disregard of system's nonlinear behaviour, especially static (Coulomb) friction. This becomes clear when changing the input amplitude between/among its boundaries 0 and 5 V. While increasing input amplitude Coulomb friction becomes negligible and thus the steady state gain k increases, see 5.5. At the same time the time constant τ decreases

parameter	value	units	variation
R	2.6	Ω	$\pm 12\,\%$
L	$180 \cdot 10^{-6}$	H	N/A
k	$7.67 \cdot 10^{-3}$	–	$\pm 12\,\%$
η_m	69	%	$\pm 5\,\%$
J_m	$4.57 \cdot 10^{-7}$	$\mathrm{kg\,m^2}$	$\pm 10\,\%$
J_l	$3 \cdot 10^{-4}$	$\mathrm{kg\,m^2}$	N/A
B_{eq}	0.01	$\mathrm{N\,m\,s\,rad^{-1}}$	$\pm 20\,\%$
η_g	90	%	$\pm 10\,\%$
n	14	–	–
K_{tacho}	0.09	$\mathrm{V\,s\,rad^{-1}}$	$\pm 2\,\%$

Table 5.1: Servo parameters

a bit but this cannot be put down to static friction. This effect is rather caused by unmodelled dynamic properties of the physical plant. Note that influence of servo's armature inductance is negligible (electromagnetic time constant $\tau_a = R/L = 0.4$ m s/rad).

Impact of model parameters variations on plant's transfer function can be described by the plant uncertainty. In 5.5 modeled and identified transfer functions are shown and uncertainty is included. The uncertainty is of multiplicative type, obtained by comparing the two utmost transfer functions according to (2.3). This gives an upper bound of the uncertainty.

The noise present in the measured velocity signal can be investigated e.g. by spectral analysis. Taking sequence of the signal in steady state (when there is no significant change in the mean) and subtracting its mean gives the noise signal. Square root of power spectral density S_{xx} of such noise is shown in 5.6. S_{xx} was obtained using FFT algorithm [38] on the autocorrelation function of noise [8, 21].

FFT faces phenomena of leakage and aliasing [8, 21]. Leakage blurs peaks in the frequency response through convolving them with functions of type $\sin(x)/x$. Loosely speaking, leakage is caused by different values at the opposite ends of FFT input signal. To reduce leakage, noise signal was weighted using Hamming time window [8]. Aliasing mirrors components with frequency greater then half of sampling frequency (here $f_s/2 = 500$ Hz) to the basic period of FFT spectra. Aliasing is usually eliminated using antialiasing filter [8, 21].

Unfortunately, antialiasing filtering is not possible here due to HW configuration of the experiment. We are left only to thorough investigation of the results by which we can conclude whether aliasing distorted the frequency spectra or not. The response of 5.6 has several frequency peaks with main peak at the frequency $f_1 = 93.7$ Hz. Consider f_1 as a basic resonant frequency. Thus can be found that the noise signal includes also 2nd (187.4 Hz) and 3rd (281.1 Hz) resonant frequencies. Peaks at 344.1 Hz and 63 Hz are the metioned aliasing mirrors of 7th and 10th resonant frequencies, respectively. Therefore

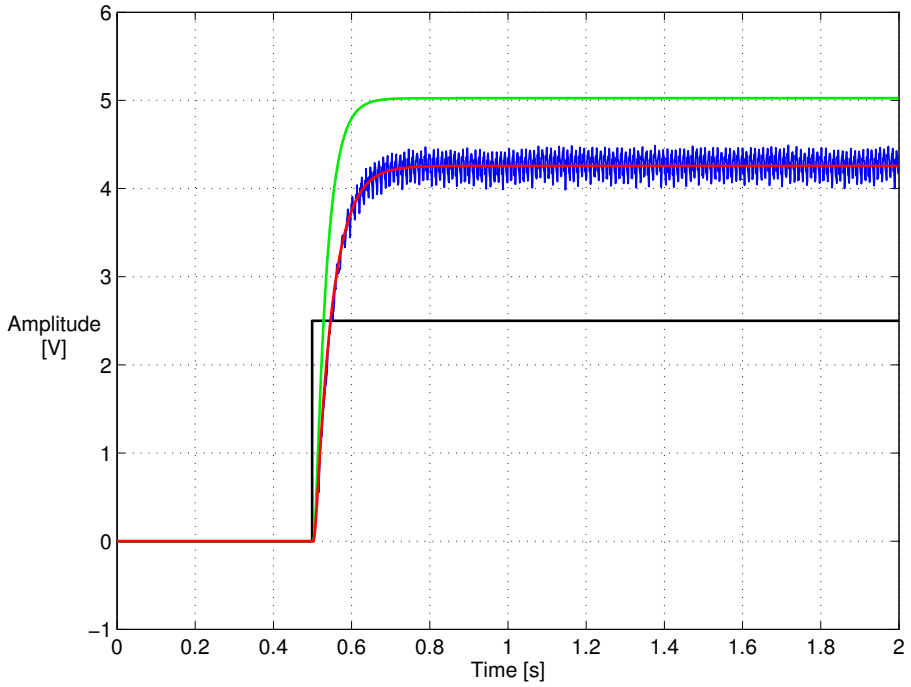

Figure 5.4: Comparison of step responses - modelled (green), measured (blue), identified (red) and the step command (black)

aliasing effects should be taken into account when gathering results from the spectral analysis.

Analyzing amplitude and frequency of several resonant frequencies their dependence on the steady state speed can be observed 5.7. Such results show that harmonic noise components are produced by the tachometer due to its irregular shape and the noise signal itself is made of white noise mixed with several discrete frequency components.

Although frequency of the noise depends on the input amplitude in a multiplicative way , it is needed (for the purposes of $\mathcal{H}_\infty$ synthesis) to develop linear noise description. This has been done by finding an upper bound for the square root of noise power spectral density S_{xx}. This upper bound can be used as an instance of the weighting filter W_3

$$W_3 = \frac{0.237\,(s\,+\,125.7)}{s\,+\,942.5}. \tag{5.7}$$

Thus we have arrived at a model of noise which is independent on the input level. At the same time this model is quite conservative as it expects presence of noise at frequency interval instead of discrete resonant frequencies.

So far only the tachometer has been studied. Now consider the other two sensors that have been designed primarily for position measurement. The optical encoder measures relative position (i.e. it has no *home position*) of the shaft. It has 4096 segments that give a resolution approximately 5'. The effects of quantization error can be analyzed using either describing function [1, 24] or stochastic description [14].

The describing function concept can be regarded as a generalization of the Nyquist

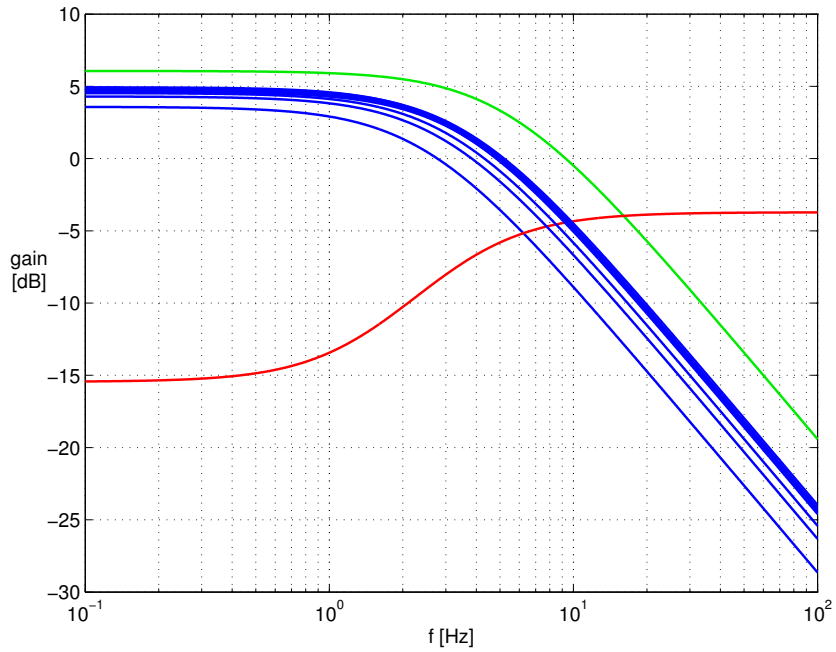

Figure 5.5: Servo model and its uncertainty - modelled transfer function (green), set of identified transfers (blue) and multiplicative model of uncertainty (red)

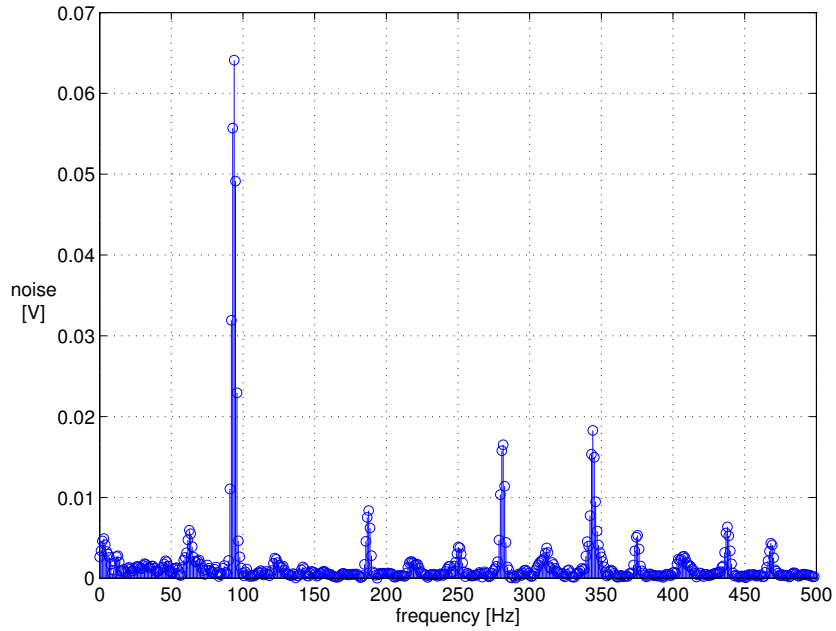

Figure 5.6: Noise FFT - Square root of noise power spectral density for $\omega = 2600$rpm

criterion and is used to test stability of systems with one nonlinearity. The critical point -1 is replaced by $-1/Y_c(A)$, where $Y_c(A)$ is the describing function of the nonlinearity. The describing function chracterizies the transmission of a sinusoidal signal with amplitude A through the nonlinearity. Evaluation of $Y_c(A)$ gives that for systems with gain

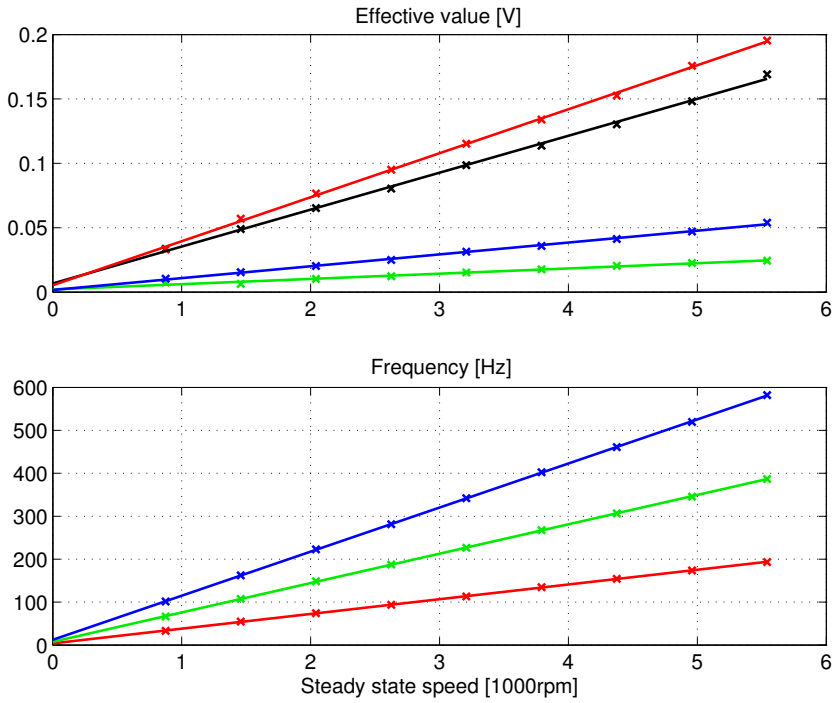

Figure 5.7: Noise as a function velocity - effective value and frequency of the first (red), second (green) and third (blue) harmonic component and effective value of the white component (black)

margine at least 1.27dB the quantization will not cause oscillations or instability.

Stochastic analysis describes the round-off error as a white noise with amplitude equally distributed over the interval $(-q/2,\ +q/2)$, where q is the quantization step. The variance σ^2 of the round-off error is then (Figure 5.8)

$$\sigma^2 = \int_{-q/2}^{q/2} \frac{x^2}{q} \mathrm{d}\, x = \frac{q^2}{12},$$

and contribution of the round-off error to the specification can be done via weighting filter

$$W_3 = \frac{q}{2\sqrt{3}}. \tag{5.8}$$

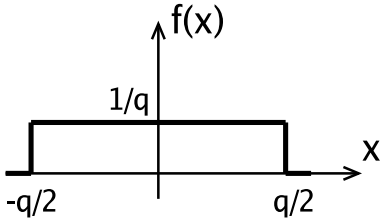

Figure 5.8: Encoder noise density

Note that the round-off error of the encoder, used for Rotary Experiment, can be disregard, if reference commands are at least 5 ° and the controller bandwidth is not too high. Both the conditions hold, the latter is forced by other control objectives.

The potentiometer output shows discontinuities, after each evolution it returns to the starting position. Thus it is suitable rather for accurate measurement and for detction of absolute position than for control tasks and position has been measured only with the encoder.

5.3 Flexible Link Modelling and Identification

In this section, model of the flexible link attached to the servo shaft will be derived using extended Hamilton's principle. During the modelling, interaction between servo and the beam will be incorporated into the model. The obtained model will be slightly modified to match the real plant behaviour.

Typically, the derivation of equations of motion for a system proceeds down two paths [31]. The first path uses Newton's equations of motion, the second path utilizes calculus of variations by defining a functional, which is based on the system energy. Hamilton's principle is the application of calculus of variations to dynamical systems. It is often referred to as the principle of least(stationary) action. Loosely speaking, it states that from a set of actions the one that minimizes variations in system's energy will be performed. The exact definition is following [25]. An action undertaken by the system between moments t_1 and t_2 must satisfy

$$\int_{-t_1}^{t_2} \delta(E_k - E_p)\, dt = 0,$$

where E_k is the total kinetic energy of the system, E_p is the potential energy of the system and δ represents the variational operator. However, this holds only for purely conservative systems and forces. Damping and external (time-dependent) forces need extension of the classical Hamilton's principle to the form ([11, 25])

$$\int_{t_1}^{t_2} \delta(E_k - E_p) + \delta\, W_{nc}\, \mathrm{d}\, t = 0 \tag{5.9}$$

called *extended Hamilton's principle*. Note that δW_{nc} is work of nonconservative forces.

Now consider a flexible link shown in 5.9. The flexible beam is controlled by torque τ, acting on a hub. The hub has inertia J_H and the beam is L long. According to the Euler-Bernoulli assumptions [9, 25], motion of the beam has two components, rotation $\theta(t)$ and transverse deformation $w(x,t)$. Any other effects of τ are neglected. θ and w are called *generalized variables* of the link's motion. Generalized variables are a minimal set

of independent variables needed to describe the system state [25]. Hence, they are known in both moments t_1 and t_2 and their respective variations are zero

$$\delta\,\theta(t_1) = \delta\,\theta(t_2) = \delta\,w(t_1) = \delta\,w(t_1). \tag{5.10}$$

Angular position α_P of a point P, that lies on the beam in the distance x from the shaft, is

$$\alpha_P(x,t) = \theta(t) + \arctan\left(\frac{w(x,t)}{x}\right). \tag{5.11}$$

Note that α_P has been expressed with respect to the frame X, Y. Assuming that the elastic deformation $w(x,t)$ is small, (5.11) can be linearized and the arc length R of P can be defined as [17]

$$R(x,t) = \theta(t)x + w(x,t).$$

Kinetic energy of a rotating flexible link undergoing transverse vibrations (all the other mechanisms of deformation are neglected) is

$$E_k = \frac{1}{2}\,J_H\,\left(\dot{\theta} + \left.\frac{\delta\dot{w}}{\delta x}\right|_{x=0}\right)^2 + \frac{1}{2}\int_0^L \left(\dot{\theta}\,x + \dot{w}\right)^2 \mathrm{d}\,x, \tag{5.12}$$

where L is length of the link and ρ is the link's mass per unit length. Potential energy due to the flexible deformation is

$$E_p = \frac{1}{2}\,EI\int_0^L \left(\frac{\partial^2 w}{\partial x^2}\right)^2 \mathrm{d}\,x, \tag{5.13}$$

where E is the Young's modulus of elasticity and I is the cross-sectional area moment of inertia. Work of external torque τ is

$$W_{nc} = \tau\,\left(\theta + \left.\frac{\partial\,w}{\partial\,x}\right|_{x=0}\right). \tag{5.14}$$

Introduction of the above expressions for E_k, E_p and W_{nc} into the extended Hamilton's principle (5.9), calculation of the respective variations $\delta\,E_k$, $\delta\,E_p$ and $\delta\,W_{nc}$ (see c.f. [11]

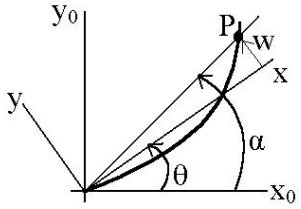

Figure 5.9: Schematic diagram of the Euler-Bernoulli beam model

for basics of variational calculus) and finally simplification with respect to (5.10) gives

$$\begin{aligned}\int_{t_1}^{t_2}\left(\tau - J_H\,\ddot{\theta} - J_H\,\left.\frac{\partial\ddot{w}}{\partial x}\right|_{x=0} + \int_0^L(\ddot{\theta}\,x+\ddot{w})\,x\,\mathrm{d}\,x\right)\delta\theta\,\mathrm{d}\,t-\\ -\int_{t_1}^{t_2}\int_0^L\left(EI\,w'''' + \rho\,(\ddot{\theta}\,x+\ddot{w})\right)\,\mathrm{d}\,x\delta w\,\mathrm{d}\,t = 0,\end{aligned} \tag{5.15}$$

where w'''' means $\frac{\partial^4 w}{\partial x^4}$.

The generalized variables θ and w are independent. Thus both the integrands in (5.15) must be identically equal to zero

$$\begin{aligned}\tau &= J_H\left(\ddot{\theta} + \left.\frac{\delta\ddot{w}}{\delta x}\right|_{x=0}\right) + \int_0^L\left(\ddot{\theta}\,x+\ddot{w}\right)\,x\,\mathrm{d}\,x,\\ 0 &= EI\,\frac{\partial^4 w}{\partial x^4} + \rho\,(\ddot{\theta}\,x+\ddot{w}).\end{aligned} \tag{5.16}$$

Note that the bending moment of the beam at its base is ([16])

$$-\,EI\,\left.\frac{\partial^2 w}{\partial x^2}\right|_{x=0} = \rho\int_0^L\left(\ddot{\theta}\,x+\ddot{w}\right)\,x\,\mathrm{d}x, \tag{5.17}$$

so the equation (5.16a) can be rewritten as

$$\tau = J_H\,\left(\ddot{\theta} + \left.\frac{\partial\ddot{w}}{\partial x}\right|_{x=0}\right) - EI\,\left.\frac{\partial^2 w}{\partial x^2}\right|_{x=0}. \tag{5.18}$$

Now the input torque τ will be inspected. The input torque, that acts on the link's hub, is somehow generated by the DC servo. To find a relation between the input voltage u of the servo and the input torque τ, return to the figure 5.3 for a while. Torque $\eta_g\,n\,\tau_m$ that is delivered by the servo to the output of the gear, must be balanced by the viscous friction $B\,\omega_l$, the inertia of motor and gear $J\,\dot{\omega}_l$ and the flexible link's input torque τ

$$\eta_g\,n\,\tau_m = J\,\dot{\omega}_l + B\,\omega_l + \tau, \tag{5.19}$$

where the gear output velocity ω_l is

$$\omega_l = \left.\frac{\partial R(x,t)}{\partial x}\right|_{x=0} = \dot{\theta} + \left.\frac{\partial\dot{w}}{\partial x}\right|_{x=0}.$$

Angular velocity $\dot{\theta}$ is the velocity of rigid motion. It denotes velocity of the link's center of mass, thus the rigid body motion is connected to the torque τ in the following way

$$\tau = (J_H + \frac{1}{3}\rho L^3)\,\ddot{\theta}. \tag{5.20}$$

So far, we have arrived at one partial differential equation (PDE) and two ordinal differential equations (ODE). The ODE (5.20) describes rigid body motion of the hub with

beam. The PDE (5.16b) describes elastic bending of the link and ODE (5.19) says, how does the bending moment influence rigid motion of the link. Now the equations need to be solved. First the PDE will be undertaken. Since equation (5.16b) is a linear homogenous PDE, the solution $w(x,t)$ is sought using the separation of variables technique [25]

$$w(x,t) = F(x)\,Q(t). \tag{5.21}$$

Substituting (5.21) into (5.16b) leads to the desired separation of variables

$$\begin{aligned} 0 &= EI\,\frac{\mathrm{d}^4F(x)}{\mathrm{d}x^4} - \rho\,\omega^2\,F(x), \\ 0 &= \frac{\mathrm{d}^2Q(t)}{\mathrm{d}t^2} + \omega^2\,Q(t). \end{aligned} \tag{5.22}$$

Notice that ω is (yet) arbitrary frequency of harmonic motion of the solution

$$Q(t) = C\,\cos(\omega\,t + \phi).$$

Introduce β as

$$\beta^4 = \frac{\omega^2\,\rho}{EI}, \tag{5.23}$$

then the general spatial solution $F(x)$ of (5.22a) is

$$F(x) = C_1\,\sin(\beta\,x) + C_2\,\cos(\beta\,x) + C_3\,\sinh(\beta\,x) + C_4\,\cosh(\beta\,x). \tag{5.24}$$

To find a particular expression for $F(x)$ (that is, find values of C_1, C_2, C_3 and C_4) corresponding to the current physical configuration, four boundary conditions (BC's) need to be introduced. They are

$$\begin{aligned} F''(L) &= 0, \\ F'''(L) &= 0, \\ F(0) &= 0, \\ EI\,F''(0) + J_H\,\omega^2\,F'(0) &= 0, \end{aligned} \tag{5.25}$$

where $F' = \frac{\partial w}{\partial x}$, $F' = \frac{\partial^2 w}{\partial x^2}$ and $F' = \frac{\partial^3 w}{\partial x^3}$.

The first BC states that there is no bending moment at tip (free end) of the link, the second BC states for zero shear force at tip of the link, the third is a geometric BC (in the hub, deformation is not assumed) and the last condition is a bit tricky one. It has arised from the equation (5.18). Note that the input torque τ has an unknown shape. Such a BC would not help at all. Instead, steady rigid motion ($\tau = 0$ and $\ddot{\theta} = 0$) has been assumed and this has given the condition (5.25d).

Now substituting (5.24) for the BC's (5.25) leads to a homogenous system of algebraic equations. This system has nontrivial solution (C_1, C_2, C_3, C_4) iff the determinant of the system matrix vanishes ([25, 26]), i.e.

$$J_H\,\beta^3\,(1 + \cos(\beta\,L)\,\cosh(\beta\,L)) + \rho\,(\sin(\beta\,L)\,\cosh(\beta\,L) - \cos(\beta\,L)\,\sinh(\beta\,L)) = 0. \tag{5.26}$$

The equation (5.26) is called *characteristic equation* related to the PDE (5.16b) and the set of BC's (5.25). The characteristic equation is a transcendental equation with no analytical solution available [9, 11, 25]. However, the characteristic equation has infinitely many solutions β_i and they can be found e.g. utilizing gradient algorithms. To do so, simple Newton method [4] has been implemented. The solution has been searched in the frequency domain, i.e. for ω (ω and β are related by (5.23), so it is possible to change domain of the algorithm). To find appropriate starting points, the frequency interval $(0, f_s/2)$ has been sampled (higher frequencies are not admissible due to the Shannon's sampling theorem, c.f. [8, 21]) and the starting points have evaluated as samples, where sign of the left side of (5.26) changes. This can be done, because the left side of characteristic equation has a shape shown in Figure 5.11.

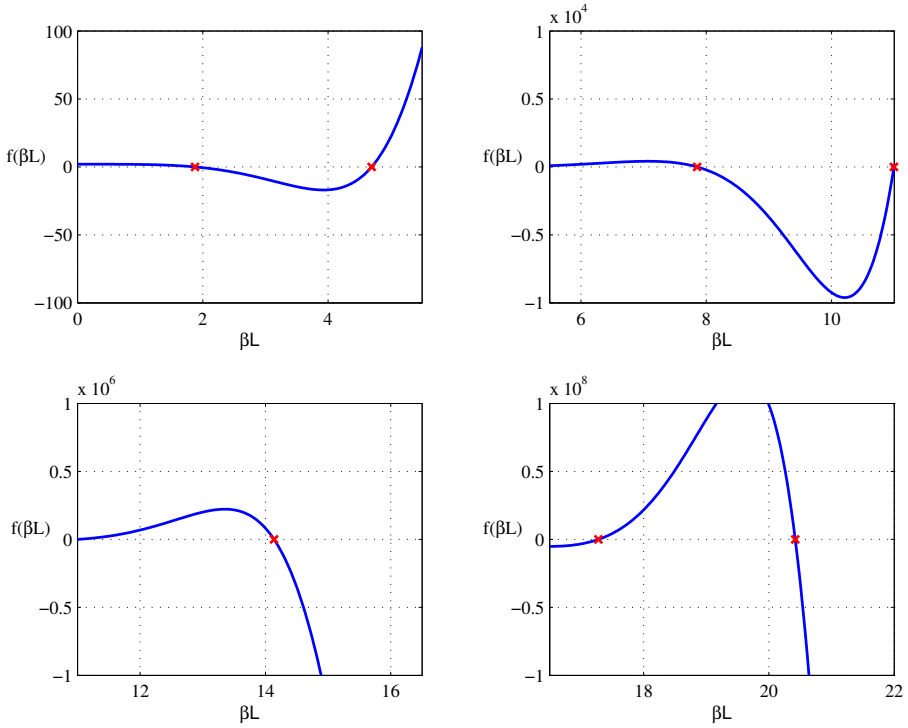

Figure 5.10: Characteristic function and its roots

As the solutions β_i to the characteristic equation (5.26) have been found, now it is possible to evaluate the coefficients C_{1i}, C_{2i}, C_{3i} and C_{4i} (the corresponding expressions are rather tedious..). They are defined up to a scaling factor. So far we have arrived at an infinite set of solutions to the PDE (5.16b) with BC's (5.25) and the solutions are

$$\begin{aligned} w_i(x,t) &= F_i(x)\,Q_i(t), \\ F_i(x) &= C_{1i}\,\sin(\beta_i\,x) + C_{2i}\,\cos(\beta_i\,x) + C_{3i}\,\sinh(\beta_i\,x) + C_{4i}\,\cosh(\beta_i\,x), \\ Q_i(t) &= \sin(\omega_i\,t), \\ \omega_i^2 &= \beta_i^4\,\frac{EI}{\rho}. \end{aligned} \tag{5.27}$$

The question is, how to incorporate this (infinite) set of solutions w_i into an expression

for the displacement $w(x,t)$. An usual way is to consider w_i as a partial mode of the displacement and to assume w in the form

$$w(x,t) = \sum_{i=1}^{n} F_i(x)\, Q_i(t). \tag{5.28}$$

This method is called *assumed modes method* (ASM) and is in strong contrast with the famous *finite element method* (FEM). ASM models the displacement as a sum of global spatialy distributed modes that take place along the whole beam. On the other hand, FEM cuts the modelled beam into pieces and locally approximates the deflection shape by simple functions (e.g. low order polynomials). Note that ASM is feasible only for geometrically simple shapes (c.f. beams). More complex structures lead to problems with global solution of PDE and characteristic equation [11, 25].

It would be kind to establish the system model, at last. The equation (5.28) shows how to incorporate modes w_i into the equation of motion (5.18). Nonetheless, during the derivation two approximations have been done and the error they have caused should be minimized. At first, to derive the BC's (5.25), τ and $\ddot{\theta}$ were set to zero. The second approximation is the silent replacement of infinite set of w_i's by finite set of n spatial modes (only 4 modes have been considered, the fourth resonant frequency at 129 Hz is already out of bandwidth). The Galerkin's method can be used to minimize the approximation errors [11, 16]. The approximation error ϵ

$$\epsilon(x,t) = \sum_{i=1}^{N} EI\, F_i''''(x)\, Q_i(t) + \sum_{i=1}^{N} \rho\, F_i(x)\, \ddot{Q}_i(t) + \rho\, \ddot{\theta}(t)\, x$$

is minimized in the following way. The error function is multiplied by one modal amplitude $F_s(x)$, integrated over the domain and set to zero

$$\int_0^L F_s(x)\, \epsilon(x)\, \mathrm{d}x = 0. \tag{5.29}$$

To solve (5.29), the *orthogonality property* of modes F_i is used [11, 27]. After some computations, (5.29) yields

$$J_H\, \ddot{\theta}\, F'(0) + \omega_s^2\, M_s\, Q_s + M_s\, \ddot{Q}_s = \tau\, F_s'(0), \tag{5.30}$$

where M_s is a constant dependent on the scale of coefficients C_1, C_2, C_3 and C_4.

Putting together (5.3), (5.19), (5.20) and (5.30) gives the final description of the servo-beam plant

$$\begin{aligned} \ddot{Q}_s + \omega_s^2\, Q_s &= \frac{F_s'(0)}{M_s} \left(\tau - J_H\, \ddot{\theta}\right) \\ \ddot{\theta} &= \frac{\tau}{J_H + \dfrac{1}{3}\rho\, L^3} \\ \tau &= \frac{\eta_g\, \eta_m\, n\, k}{R}\, u - \left(B + \frac{\eta_g\, \eta_m\, n^2\, k^2}{R}\right) \omega_l - J\, \dot{\omega}_l. \end{aligned} \tag{5.31}$$

Measured velocity ω_l and tip velocity ω_{tip} are (Figure 5.9)

$$\begin{aligned} \omega_l &= \dot{\theta} + \textstyle\sum_{s=1}^{N} F_s'(0)\,\dot{Q}_s, \\ \omega_{tip} &= \dot{\theta} + \textstyle\sum_{s=1}^{N} F_s'(L)\,\dot{Q}_s. \end{aligned} \tag{5.32}$$

As damping forces have not been taken into account when an expression for the work of nonconservative forces W_{nc} has been constructed, the resulting equations of motion (5.31) are undamped. On the other hand, real plant exhibits damping (see Figure5.11). According to with [9] modal damping ξ_s can be easily included in the model (5.31)

$$\ddot{Q}_s + 2\,\xi_s\,\omega_s\,\dot{Q}_s\omega_s^2\,Q_s = \frac{F_s'(0)}{M_s}\,\left(\tau - J_H\,\ddot{\theta}\right).$$

This leads to the same result as if the damping forces have been derived from the Rayleigh dissipation function [25].

The equations of motion (5.31) would lead to complicated state-space model. The situation can be simplified assuming that the beam deflection at the end with hub is negligible. Then the measured velocity ω_l is approximately the rigid motion velocity θ,

$$\omega_l = \dot{\theta} + \left.\frac{\partial \dot{w}}{\partial x}\right|_{x=0},$$

and one possible state-space model of the plant is

$$\begin{aligned} x_1 &= \theta, x_2 = \dot{\theta}, x_3 = Q_1, x_4 = \dot{Q}_1, x_5 = Q_2, x_6 = \dot{Q}_2, \ldots \\ y_1 &= \omega_l, y_2 = \sigma \\ A &= \begin{pmatrix} 0 & 1 & 0 & 0 & 0 & 0 & 0 & 0 & \ldots \\ 0 & -B/J & E\,I\,F_1''(0)/J & 0 & E\,I\,F_2''(0)/J & 0 & E\,I\,F_3''(0)/J & 0 & \ldots \\ 0 & 0 & 0 & 1 & 0 & 0 & 0 & 0 & \ldots \\ 0 & -F_1'(0)\,B & -\omega_1^2 + E\,I\,F_1'(0)\,F_1''(0) & -2\,\xi_1\,\omega_1 & E\,I\,F_1'(0)\,F_2''(0) & 0 & E\,I\,F_1'(0)\,F_3''(0) & 0 & \ldots \\ 0 & 0 & 0 & 0 & 0 & 1 & 0 & 0 & \ldots \\ 0 & -F_2'(0)\,B & E\,I\,F_2'(0)\,F_1''(0) & 0 & -\omega_2^2 + E\,I\,F_2'(0)\,F_2''(0) & -2\,\xi_2\,\omega_2 & E\,I\,F_2'(0)\,F_3''(0) & 0 & \ldots \\ \vdots & & & & & & & \vdots & \end{pmatrix} \\ B &= \begin{pmatrix} 0 & k_1/J & 0 & k_1\,F_1'(0) & 0 & k_1\,F_2'(0) & 0 & k_1\,F_3'(0) & \ldots \end{pmatrix}^{\mathrm{T}} \\ C &= \begin{pmatrix} 0 & 1 & 0 & F_1'(0) & 0 & F_2'(0) & 0 & F_3'(0) & \ldots \\ 0 & 0 & -E\,I\,F_1''(0) & 0 & -E\,I\,F_2''(0) & 0 & -E\,I\,F_3''(0) & 0 & \ldots \end{pmatrix} \\ D &= \begin{pmatrix} 0 \\ 0 \end{pmatrix}, \end{aligned}$$

where σ is strain measured by strain gauge.

The flexible link's parameters in (5.33) are of two types. L, E, I, ρ and J_H are the structural parameters needed to calculate the other parameters ω_s, $F_s(0)$, $F_s(L)$, $F_s'(0)$

etc. However, only $L = 30cm$ is known! (it should be remarked, that Quanser did not include promised user manual to the SRV02 package and it was impossible to find it on the quanser web pages [30] either)

On the other hand, it is possible to at least estimate the values of unknown E, I, ρ and J_H. The flexible beam is made of aluminium. So, typical values for E and ρ_m have taken from [11]. ρ_m states for mass density, while ρ used above is the cross-sectional desntiy. Thus the cross section A has been measured and ρ estimated as $\rho = \rho_m/A$.

To find out, what value I could have, the flexible beam has been removed from the hub and put into a press screw. Response on initial excitation has been measured (Figure **??**) and the dominant resonant frequency ω_D and respective damping ξ_D have been found. I has been estimated using (5.23) to be

$$I = \frac{\omega^2 \rho}{\beta_D^4 E},$$

where β_D is the first solution of characteristic equation (5.26) for the setup with press screw. In this cas J_H is regarded to be infintely high [9] and (5.26) degrades to

$$1 + \cos(\beta L) \cosh(\beta L).$$

Thus β_D depends only on known length L.

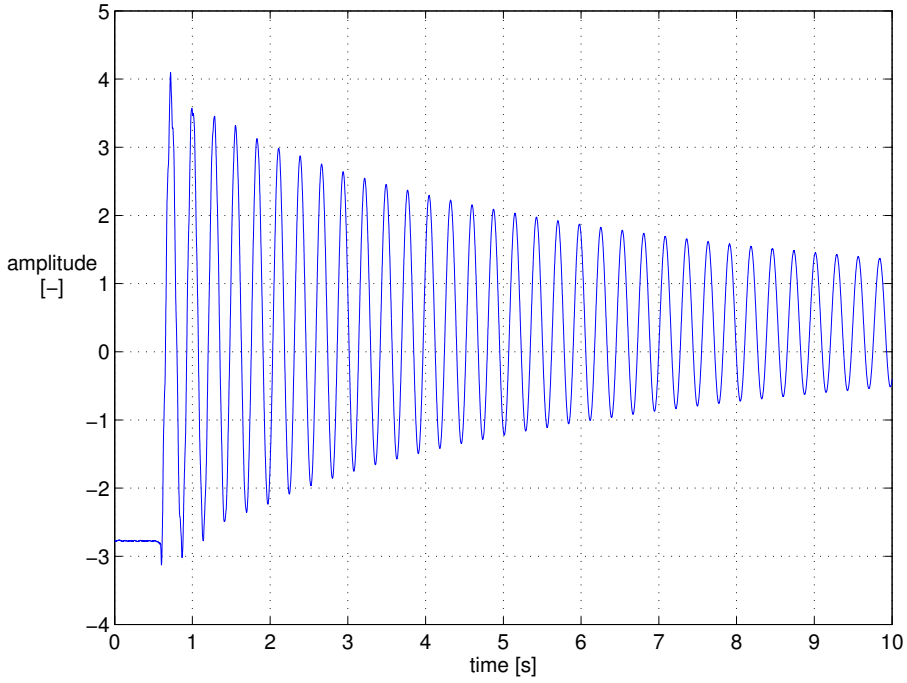

Figure 5.11: Measured strain for clamped-free beam

To estimate J_H, responses of the plant (beam attached to the servo again) on harmonic input have been measured and evaluated. Data from the tachometer have been processed through selective resonant filter tuned on the input signal frequency, so as to minimize

the effects of tacho ripple (see section 5.2). The best value of J_H has been iteratively searched. After some iterations it has become clear that to fit the measured frequency response, it would be necessary to slightly change values of the other parameters too. The final parameter values are shown in Table 5.2. Comparison of measured and identified frequency responses for both the tachometer and strain gauge are shown in Figure 5.12. Note that frequency of the input signal must be under approximately 40 Hz. This limits the bandwidth in which the identified model can be accurate. Beyond approximately 20 Hz the model is not much reliable.

parameter	value	units
E	$6.9 \cdot 10^{10}$	$N\,m^{-2}$
I	$2.6 \cdot 10^{-12}$	m^4
ρ	$54 \cdot 10^{-3}$	$kg\,m^{-1}$
J_H	$31 \cdot 10^{-3}$	$kg\,m^2$

Table 5.2: Beam parameters

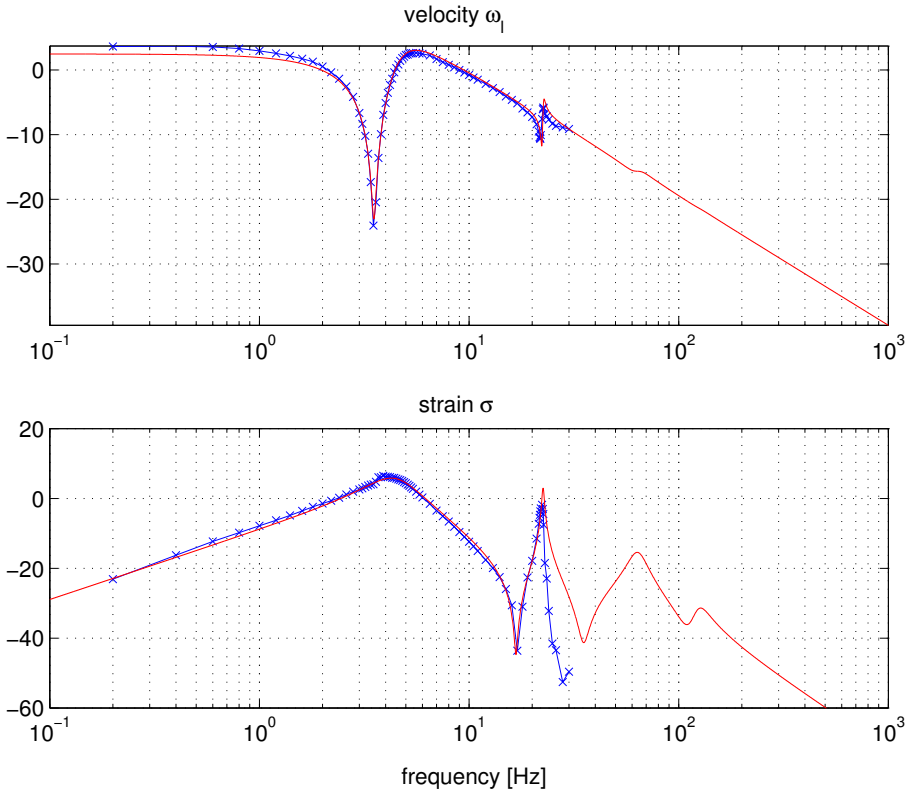

Figure 5.12: Comparison of measured(blue) and identified(red) frequency responses

5.4 Controller Design and Experimental Results

Problem of the flexible link tip position control is somewhat tricky. The plant is equipped only with sensors located at (near) the hub of the link. On the other hand it is desired to control position of the opposite end. Such a control problem is often reffered to as *noncollocated control* [9]. To demonstrate this problem, two controllers will be designed. The first has the 2-loop configuration of Figure 5.13. The inner loop is derived from the tachometer and the outer loop is derived from the optical encoder. Thus it is possible to control velocity ω_l and position $= \theta_l$ of the hub. Note that steady position at the hub does not assure steady position at the tip of the beam. On the contrary, poor results will be shown.

The positioning control problem can be formulated as: arrive at asymptotic tracking of constant position reference and minimize sensitivity to output disturbances while respecting limitations on the input voltage. It is useful to recall the limits set on u - amplitude of u should not exceed 5V and u should be attenuated enough at frequencies beyond 50Hz.

The 2-loop controller divides responsibility for the actual control goals between the inner and the outer loop. The inner velocity loop "smoothens" resonances of the plant and assures wide bandwidth. Note that except for the limiations of u also the ripple noise and model uncertainty limit the achievable bandwidth. After several iterations, the following weighting filters have been found the best

$$\begin{aligned} W_1 &= 0.953\,\frac{s+9.935}{s+0.09473}, \\ W_2 &= 0.707, \\ W_3 &= 10^4\,\frac{(s+58.57)^2}{(s+6966)^2}. \end{aligned}$$

Input disturbances are not considered (noise of the input voltage is neglected). Problem with nonproper W_3 is solved by a pair of high-frequency poles.

The outer position loop assures asymptotic tracking and reduces sensitivity to disturbances. The achievable bandwidth is limited by the plant model uncertainty. It would be tedious to derive an uncertainty model of the inner closed-loop system based on original uncertainty of the plant. Instead, best weighting filters have been found iteratively

$$\begin{aligned} W_1 &= 1.633\,\frac{s+13.33}{s}, \\ W_2 &= 4, \\ W_3 &= 2.453\,\frac{s+25.13}{s+87.2}. \end{aligned}$$

To shape the step response, prefilter

$$C_p = 84.3\,\frac{(s^2+11.4s+361)}{(s+251.3)\,(s^2+8.8s+121)}$$

has been used.

Resulting step responses are shown in Figure 5.14. Asymptotic tracking has been obtained and prefilter has limited the overshoot. However, the closed-loop system is very sensitive to output disturbances. The second controller should cure this. According to (5.32), the tip velocity can be estimated from the strain gauge and tachometer measurement

$$\omega_{tip} = \omega_l + \lambda\,\sigma,$$

where σ is strain measured by the strain gauge and λ is a function of the spatial coefficients $F_s(0)$, $F_s'(0)$, $F_s''(0)$, $F_s(L)$, $F_s'(L)$, $F_s''(L)$, $s = 1, 2, ..$ **??**. The following weighting filters have been found to give best results for the velocity loop

$$\begin{aligned} W_1 &= 1.91\,\frac{s+10.93}{s+0.1042}, \\ W_2 &= 0.5, \\ W_3 &= 2.453\,\frac{(s+68.34)^2}{(s+8126)^2}. \end{aligned}$$

Note that both velocity loops have similar controllers, but the noncollocated directly considers the deflection measured by the strain gauge and thus it offers better disturbance attenuation. Improvement of the step response in comparison with the original step response is shown in Figure 5.15. Well, due to lack of time, I stopped right here and did not complete the design with the outer position loop. But it is believed that this could be done similarly to the collocated position control and finally obtain 2-loop controller with improved disturbance attenuation.

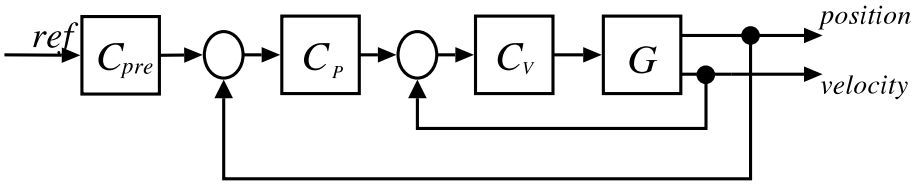

Figure 5.13: Closed loop configuration

5.5 Conclusions

In this chapter the servo plant with attached flexible link has been modelled and identified. The identification procedure has given model that describes the real plant very well, at least at the key frequency region around the first resonant frequency. On the other hand time spent on system modelling has been missed during the controller design phase. Only the collocated controller has been completed. This controller assures asymptotic tracking of constant reference and (with a prefilter) it gives sufficiently smooth time response.

The design of noncollocated controller, that would efficiently attenuate possible output disturbances, was fulfilled only partialy - as a velocity controller. Note that the

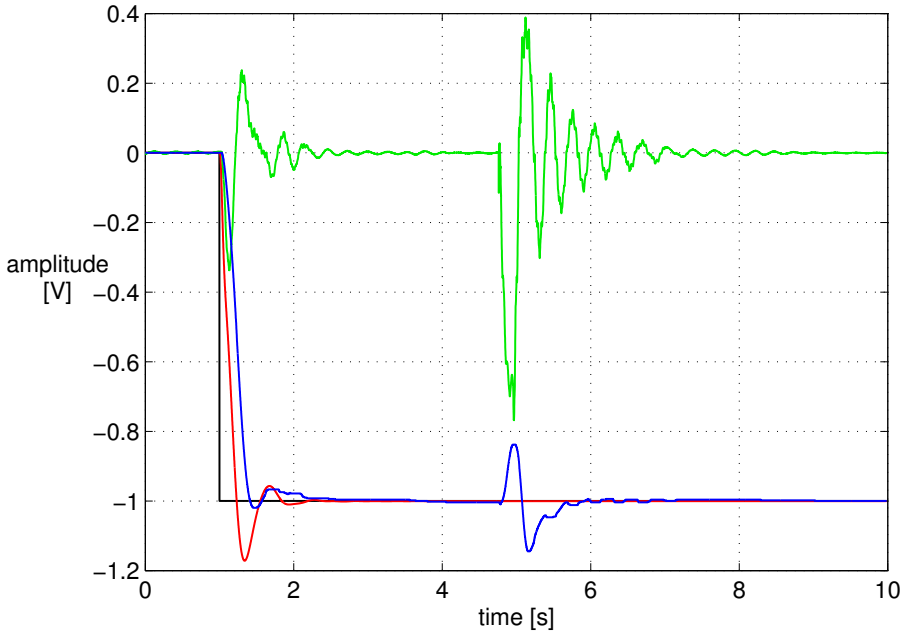

Figure 5.14: Closed loop time responses - position step response without prefilter(red) and with prefilter(blue) and strin gauge step response(green). At the time $t = 5$s heavy output disturbance occured (strike by a hand)

noncollocated velocity controller has been designed using weighting filters similar to the weights for collocated controller. One can expect that it would be possible to design the full noncollocated position controller.

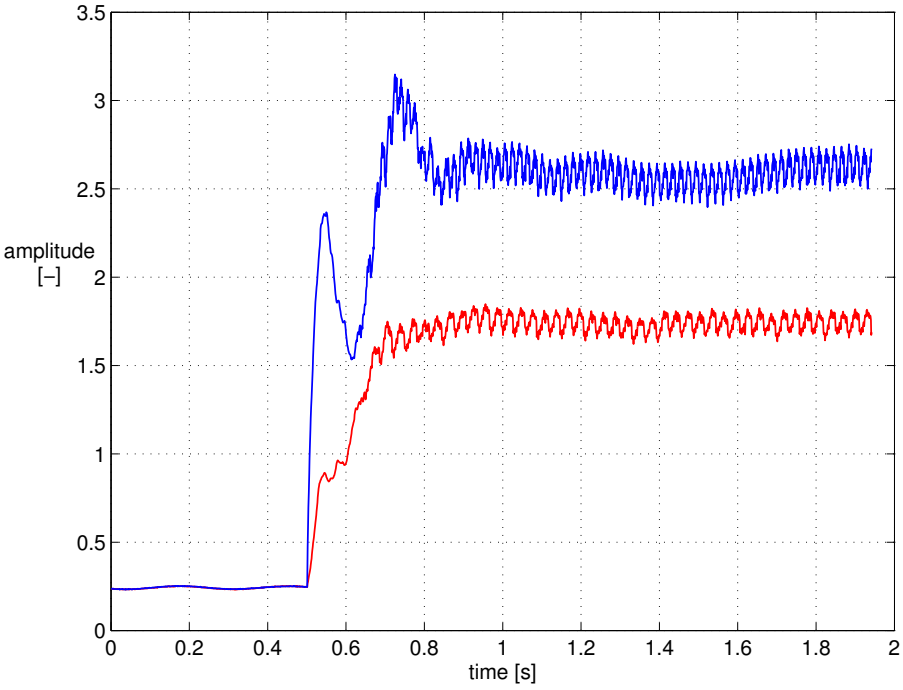

Figure 5.15: Noncollocated control - step response

Chapter 6

Conclusions

In this thesis the $\mathcal{H}_\infty$ optimization approach has been used to define and solve control problems. Common ways how to convert typical control objectives to frequency domain specifiction have been summarized. Several remarks on their feasibility have been concluded. These remarks have helped to explain some phenomena faced when designing the controllers.

Two situations have been considered. The VLT position control problem and the Quanser Rotary Experiment. Both plants have similar overall behaviour - 2nd order low-pass filter with several resonant frequencies. Model of the VLT was given by the ESO engineer and thus the VLT problem has been reduced only to controller design. After a carefull inspection of the given model 2-DOF controller structure has been chosen. The control objectives have been found too conflicting to get good performance with 1-DOF controller only. After many iterations a controller that beats the existing solution has been found. It has been concluded that the desired performance improvement sets tighter limitations on the accuracy of measurement.

The Rotary Experiment has offered an opportunity to go through the complete controller design including modelling and identification and testing on the real plant. Extensive work on the plant modelling and identification has been done, resulting in a model that matches the real plant fairly well at key frequency range. It has been noted, that the tip positioning is a noncollocated control problem. Collocated controller has been designed and it has been verified that, though it has stabilized the closed loop and it has lead to smooth step tracking, the resulting closed loop system is very sensitive to disturbances at the tip. Noncollocated controller design has not been completed due to lack of time. However, it is believed that $\mathcal{H}_\infty$ synthesis of such controller is possible.

During the VLT controller design a GUI for model order reduction has been often used. The GUI has been implemented as a part of this work and its aim has been to simplify and speed up the process of model reduction. The GUI has proven its worth while it has helped to reveal, that the given VLT model has not been as reliable as it was originally thought. This observation lead to a conclusion that, in the real situation, some control trade-offs could be less pronounced.

Bibliography

[1] Astrom, K. J. – Wittenmark, B., editor. *Computer-controlled systems, theory and design*. New Jersey: Prentice Hall, 1997.

[2] Balas, G. J. – Doyle, J. C. – Glover, K. – Packard, A. – Smith, R. μ–analysis and synthesis toolbox, 1995.

[3] Bely, P.-Y., editor. *The Design and Construction of Large Optical Telescopes*. Springer, 2003. ISBN 0-387-95512-7.

[4] Boyd, S. – Vandenberghe, L. *Convex Optimization*. Cambridge, UK: Cambridge University Press, 1st edition, 2004. ISBN 0-521-83378-7.

[5] Brunetto, E. et al. OWL opto-mechanics, phase a. In *Proc. SPIE 5489*, 2004.

[6] Chiang, R. Y. – Safonov, M. G. Robust control toolbox, 1992.

[7] Damen, A. – Weiland, S. *Robust Control*. Eindhoven University of Technology, Eindhoven, 2002.

[8] Davídek, V. – Sovka, P. *Číslicové zpracování signálů a implementace*. Praha: Vydavatelství ČVUT, 2nd edition, 2002. ISBN 80-01-02483-0.

[9] De Luca, A. – Caiano, V. – Del Vescovo, D. Experiments on rest-to-rest motion of a flexible arm. In 8th *International Symposium on Experimental Robotics*, Sant'Angelo d'Ischia, Italy, 2002.

[10] Doyle, J. C. – Francis, B. A. – Tannenbaum, A. R. *Feedback Control Theory*. New York: Macmillan, 1992.

[11] Egeland, O. – Gravdahl, J. T. *Modelling ans Simulation ofr Automatic Control*. Trondheim, Norway: Marine Cybernetics, 2nd edition, 2003. ISBN 82-92356-01-0.

[12] Erm, T. – Hurák, Z. – Bauvir, B. Time to go $\mathcal{H}_\infty$? In *Proceedings of SPIE International Symposium Astronomical Telescopes*, Glasgow, Scotland, 2004.

[13] Eso – the european southern observatory homepage [online]. ⟨`http://www.eso.org`⟩, 2005. [2005-01-19].

[14] Franklin, G. F. – Powell, J. D. – Workman, M. *Digital control of dynamic systems.* Addison Wesley, 3rd edition, 1997. ISBN 0-201-82054-4.

[15] Gawronski, W. K. *Dynamics and control of structures.* New York: Springer Verlag, 1st edition, 1998. ISBN 0-387-98527-1.

[16] Ge, S. S. – Lee, T. H. – Hong, F. Adaptive control of a distributed-parameter flexible beam. In *Proceedings of the* 4th *Asian Conference on Robotics and its Applications (ACRA'01)*, Singapore, June 2001.

[17] Ghanekar, M. *Ph. D. Thesis: Scaling Laws for Linear Controllers of Dynamically Equivalent Single Flexible Link Manipulators.* Waterloo, Canada: University of Waterloo, 1994.

[18] Gugercin, S. – Antoulas, A. C. A survey of model reduction by balanced truncation and some new results. *International Journal of Control, Volume 77, Issue 8*, February 2004.

[19] Havlena, V. – Štecha, J. *Moderní teorie řízení.* Praha: Vydavatelství ČVUT, 2st edition, 2000.

[20] Henrion, D. – Prieur, C. – Tliba, S. Improving conditioning of polynomial pole placement problems with application to low-order controller design for a flexible beam. *LAAS-CNRS Research Report No. 04163*, February 2004.

[21] Hlaváč, V. – Sedláček, M. *Zpracování signálů a obrazů.* Praha: Vydavatelství ČVUT, 1st edition, 2001. ISBN 80-01-02114-9.

[22] Horáček, P. *Systémy a modely.* Praha: Vydavatelství ČVUT, 2nd edition, 2000. ISBN 80-01-01923-3.

[23] Hromčík, M. – Hurák, Z. – Šebek, M. Robustní řízení [online]. ⟨`http://dce.felk.cvut.cz/ror`⟩, 2004. [cite 2004-11-11].

[24] John, J. *Systémy a řízení.* Praha: Vydavatelství ČVUT, 1st edition, 1999. ISBN 80-01-01474-6.

[25] Junkins, J. J. – Kim, Y. *Introduction to Dynamics and Control of Flexible Structures.* Washington,D.C.: AIAA, 1993. ISBN 1-56347-054-3.

[26] Krajník, E. *Maticový počet.* Praha: Vydavatelství ČVUT, 1st edition, 2000. ISBN 80-01-01723-0.

[27] Kuo, Ch. - F. J. – Lin, S. Ch. Modal analysis and control of a rotating euler-bernoulli beam, part i: Control system analysis and controller design. *Mathematical and computer modelling, volume 27*, March 1998.

[28] Kučera, V. *Discrete Linear Control.* John Wiley and Sons, 1979.

[29] Kwakernaak, H. *Design Methods for Control Systems.* Technical University Delft, 2003.

[30] The quanser homepage [online]. ⟨`http://www.quanser.com`⟩, 2005. [2005-01-19].

[31] Robinett, R. D. et al. *Flexible robot dynamics and controls.* New York: Kluwer Publishing, 3rd edition, 2002. ISBN 0-306-46724-0.

[32] Schipani et al. VST telescope dynamic analysis and position control algorithms. In *Proceedings of 8th International Conference on Accelerators and Large Experimental Physics Control Systems*, San Jose, California, 2001.

[33] Skogestad, S. – Postlethwaite, I. *Multivarible Feedback Control.* Chichester: John Wiley and Sons, 1st edition, 1996.

[34] Štecha, J. – Havlena, V. *Teorie dynamických systémů.* Praha: Vydavatelství ČVUT, 2nd edition, 2002. ISBN 80-01-01971-3.

[35] Weiland, S. Model approximation of dynamical systems. ⟨`http://www.cs.ele.tue.nl/sweiland/modred.pdf`⟩, 2004. [cite 2005-01-19].

[36] Zhou, K. *Essentials of Robust Control.* New Jersey: Prentice-Hall, 2st edition, 1998.

[37] Control system toolbox. The Mathworks, Inc. [online]. ⟨`http://www.engin.umich.edu/group/ctm`⟩, 1992. [cite 2004-08-30].

[38] The mathworks homepage. The Mathworks, Inc. [online]. ⟨`http://www.mathworks.com`⟩, 2005. [2005-01-23].

List of Figures

List of Tables

Appendix

The following function implements model approximation procedure called by the Order Reduction GUI.

```
function NewModel = reduction(OldModel,method,type,new_order,tolerance);
warning off all;
switch method
    case 'modred'
        TempModel = balreal(minreal(OldModel,0.001));
        [tmp_order temp_order] = size(TempModel.a);
        NewModel = modred(TempModel,new_order+1:temp_order,type);
    case 'balmr'
        if OldModel.Ts>0,
            TempModel = d2c(OldModel,'tustin');
        else
            TempModel = OldModel;
        end
        switch type
            case 1
                [NewModel,totbnd,svh] = balmr(TempModel,1,new_order);
            case 2
                [NewModel,totbnd,svh] = balmr(TempModel,2,tolerance);
        end
    case 'schmr'
        if OldModel.Ts>0,
            TempModel = d2c(OldModel,'tustin');
        else
            TempModel = OldModel;
        end
        switch type
            case 1
                [NewModel,totbnd,svh] = schmr(TempModel,1,new_order);
            case 2
                [NewModel,totbnd,svh] = schmr(TempModel,2,tolerance);
        end
    case 'obalreal'
```

```
    if OldModel.Ts>0,
        TempModel = d2c(OldModel,'tustin');
    else
        TempModel = OldModel;
    end
    TempModel = minreal(TempModel,0.001);
    [Aobal,Bobal,Cobal,go,to] =
           obalreal(TempModel.a,TempModel.b,TempModel.c);
    NewModel=ss(Aobal(1:new_order,1:new_order),
           Bobal(1:new_order,:),Cobal(:,1:new_order),TempModel.d);
case 'ohklmr'
    if OldModel.Ts>0,
        TempModel = d2c(OldModel,'tustin');
    else
        TempModel = OldModel;
    end
    switch type
        case 1
            [NewModel,totbnd,hsv] = ohklmr(TempModel,1,new_order);
        case 2
            [NewModel,totbnd,hsv] = ohklmr(TempModel,2,tolerance);
    end
case 'ohkapp'
    if OldModel.Ts>0,
        TempModel = d2c(OldModel,'tustin');
    else
        TempModel = OldModel;
    end
    switch type
        case 1
            [NewModel,totbnd,hsv] = ohkapp(TempModel,1,new_order);
        case 2
            [NewModel,totbnd,hsv] = ohkapp(TempModel,2,tolerance);
    end
case 'bstschml'
    if OldModel.Ts>0,
        TempModel = d2c(OldModel,'tustin');
    else
        TempModel = OldModel;
    end
    TempD = TempModel.d;
    [Rows Cols] = size(TempModel.d);
    if rank(TempModel.d)<Rows && rank(TempModel.d)<Cols,
        TempModel.d = 1e-006*eye(Rows,Cols);
```

```
        end
        switch type
            case 1
                [NewModel,aug,svh] = bstschml(TempModel,1,new_order);
            case 2
                [NewModel,aug,svh] = bstschml(TempModel,2,tolerance);
        end
        if rank(TempModel.d)<Rows && rank(TempModel.d)<Cols,
            NewModel.d = TempD;
        end
    case 'bstschmr'
        if OldModel.Ts>0,
            TempModel = d2c(OldModel,'tustin');
        else
            TempModel = OldModel;
        end
        TempD = TempModel.d;
        [Rows Cols] = size(TempModel.d);
        if rank(TempModel.d)<Rows && rank(TempModel.d)<Cols,
            TempModel.d = 1e-006*eye(Rows,Cols);
        end
        switch type
            case 1
                [NewModel,aug,svh] = bstschmr(TempModel,1,new_order);
            case 2
                [NewModel,aug,svh] = bstschmr(TempModel,2,tolerance);
        end
        if rank(TempModel.d)<Rows && rank(TempModel.d)<Cols,
            NewModel.d = TempD;
        end
    case 'srelbal'
        sssystem = balreal(ss(OldModel));
        [A,B,C,D] = ssdata(sssystem);
        [z,p,k] = ss2zp(A,B,C,D);
        system = zp2sys(z,p,k);
        [stochbal,relsv,sysfact] = srelbal(system);
        [A,B,C,D] = unpck(stochbal);
        ssstochbal = ss(A,B,C,D);
        stochred = strunc(stochbal,new_order);
        [A,B,C,D] = unpck(stochred);
        NewModel = ss(A,B,C,D);
end
warning on all;
```